Enhanced Targeting of Cellular Delivery through Reactive Oxygen Species (ROS)-Activated Liposomes with Boronate-Caged Arginylglycylaspartic acid (RGD) Lipid

A Thesis Presented for the
Master of Science
Degree
The University of Tennessee, Knoxville

Michael Temitope Kadiri
December 2024

Acknowledgments

First and foremost, I want to sincerely thank God for giving me the strength and perseverance to reach this milestone. His guidance has been my foundation, and I am grateful as I prepare to step into the next chapter of my life. Also, I am deeply grateful to my advisor Dr. Michael Best for giving me the incredible opportunity to be part of his research group. The lessons I've learned under your mentorship have not only shaped me into a more confident scientist but have also equipped me with skills I will carry throughout my career, a career that you have significantly influenced.

I also express my sincere gratitude to my past and present group members. Dr. Jinchao Lou, your ability to challenge my thinking and push me to explore ideas beyond the obvious has been transformative. Dr. Christelle Ancajas, your readiness to provide a listening ear during challenging times has been a significant source of solace. I wish to thank Dr. Ruhani Sagar, Dr. Megan Qualls, and Justin Kirby for their invaluable guidance when I joined the lab. Thank you to the current members - Smith Brooke, Kazi Shahriar, Mayesha Mustapha, Annaleena Hansen, Mahbub Ullah, and Rob Maraski- for cultivating a collaborative and welcoming atmosphere. I would also like to express my sincere gratitude to my committee members, Dr. Thanh Do and Dr. Joshua Baccile, whose invaluable guidance and support left a lasting impact on my academic journey.

To my family, words cannot express how thankful I am for your constant moral support and love, especially when I needed it most. You have been my cornerstone throughout this entire journey.

To my dear friends - Kelechi, Emmanuel, Christine, Joy, Kenny, Morris, Kingsley, Jerry, Joshua, Opeyemi, Godwin, Bukola, Iyanuoluwa, Boris, Tawakalitu, Mr. and Mrs. Roberts, Deborah, and Wilson – thank you for being my pillars of strength during my time here. Whether through your constant calls and texts to check in on me, late-night study sessions, reminding me when to take a break and recharge, or the encouragement you provided during moments of self-doubt, you have shown me unwavering friendship and support. Each of you contributed in your unique way, and for that, I am forever grateful. You are all truly amazing, and I could not have done this without you.

Abstract

Liposomes are widely recognized for their roles in drug delivery systems due to their ability to encapsulate hydrophilic and hydrophobic drugs. However, their lack of selectivity and limited targeting of diseased cells often result in off-target effects, reducing their overall therapeutic efficacy. Additionally, achieving sufficient liposomal uptake by diseased cells remains a significant challenge. Surface modification is a valuable strategy that have been employed to enhance liposomal drug delivery. This thesis will detail the design and synthesis of a boronate-caged arginyl glycyl aspartic acid (RGD) lipid aimed at improving liposome specificity and uptake through activation by reactive oxygen species (ROS). The RGD peptide was chosen for its high affinity for integrin receptors, which are overexpressed on cancer cells. Once activated by ROS, the uncaged RGD-lipid is expected to enhance receptor-mediated endocytosis, hence promoting the uptake of liposomes into cancer cells. Significant progress has been made in synthesizing key intermediates, providing a solid foundation for completing the final ROS-responsive RGD lipid. Upon completion, the compound will be thoroughly characterized to assess its activity. This research advances the development of more effective liposome-based drug delivery systems. It provides valuable insights into boronate caging chemistry, particularly its application to amino acids like arginine in the design of RGD-lipids.

Table of Contents

Chapter 1. Background 1
1.1 Introduction to Liposomes 1
1.2 Liposomes in drug delivery 4
1.2.1 Overview of smart drug delivery systems 4
1.2.2 Liposome-based drug delivery systems 4
1.2.3 Surface modifications of liposomes 6
1.3 Integrins 9
1.3.1 RGD peptides and role in cellular targeting 9
1.4 Reactive oxygen species (ROS) in drug delivery 11
1.4.1 Introduction to ROS 11
1.4.2 Sources of ROS Generation 12
1.4.3 Mechanisms of nanoparticle-mediated ROS generation 12
1.4.4 ROS-responsive polymeric nanoparticles 14
1.5 Summary 15
Chapter 2. Enhanced Targeting of Cellular Delivery through ROS – Activated liposomes Utilizing a Boronate-Caged RGD Lipid 16
2.1 Overview and rationale of project 16
2.2 Previous Research on ROS-responsive liposomes 17
2.3 Design of ROS-responsive RGD lipid 20
2.4 Synthesis Details of ROS-responsive RGD-lipid 23
2.5 Conclusion 31
2.6 Experimental 32
2.6.1 General Considerations 32
2.6.2 Synthetic procedures 32
References 40
Appendix 49
Vita 63

List of Figures

Figure 1.1: Essential components of glycerophospholipids structure 2
Figure 1.2: Liposomes classification according to their lamellarity and size. 3
Figure 1.3: A visual representation of various smart nanocarrier types used for drug delivery. 5
Figure 1.4: Cartoon depicting various types of liposomes and their functional modification. 7
Figure 1.5: A diagrammatic representation of different states of integrin activation. 10
Figure 1.6: Schematic representation of the sources of ROS in biological system. 13
Figure 2.1: Cartoon showing boronate cleavage present in lipid 7 to form lipid 8……...22
Figure 3.1: ^{1}H NMR of 3…… ……49
Figure 3.2: ^{13}C NMR of 3 50
Figure 3.3: ^{1}H NMR of 4..... 51
Figure 3.4: ^{13}C NMR of 4 52
Figure 3.5: ^{1}H NMR of 9..... 53
Figure 3.6: ^{13}C NMR of 9 54
Figure 3.7: ^{1}H NMR of 10..... 55
Figure 3.8: ^{13}C NMR of 10 56
Figure 3.9: ^{1}H NMR of 11..... 57
Figure 3.10: ^{13}C NMR of 11..... 58
Figure 3.11: ^{1}H NMR of 5..... 59
Figure 3.12: ^{13}C NMR of 5 60
Figure 3.13: ^{1}H NMR of 14..... 61
Figure 3.14: ^{13}C NMR of 14 62

List of Schemes

Scheme 1: Synthesis of ROS-responsive lipid 1a 18
Scheme 2: Synthesis of a caged guanidine lipid 2a 19
Scheme 3: A caged RGD-lipid 7 that cleaves in the presence of hydrogen peroxide 21
Scheme 4: Original synthetic route for lipid 7 24
Scheme 5: Synthesis of caged terminal carboxylic acid, lipid 22 26
Scheme 6: Synthetic route for lipid 18 27
Scheme 7:Synthetic route for the linker, boronate cage and lipid tail 29
Scheme 8: Synthetic trial of boronate caging of guanidine nitrogen on arginine 30

List of Abbreviations

DIEA	*N*,*N*-Diisopropylethylamine
DMAP	4-dimethylaminopyridine
µM	Micromolar
Boc	*tert*-Butylcarbamate
CuAAC	copper-catalyzed azide-alkyne cycloaddition
DMF	*N*,*N*-Dimethylformamide
DOPE	Dioleoylphosphatidylethanolamine
DOX	Doxorubicin
ECM	Extracellular matrix
eq	equivalent
ER	Endoplasmic reticulum
FDA	Food and Drug administration
Fmoc	fluorenylmethoxylcarbonyl
GUV	Giant unilamellar vesicles
HA	Hyaluronic acid
HOBr	Hypobromous acid
IC_{50}	Half-maximal inhibitory value
IMD	Integrin-mediated death
LUV	Large unilamellar vesicles
mL	Milliliters
MLV	Multilamellar vesicles
MVV	Multivesicular vesicles
NADPH	Nicotinamide adenine dinucleotide phosphate hydrogen
nM	nanomolar
NMR	Nuclear magnetic resonance
NP	Nanoparticles
OH	Hydroxy
ONOO	Peroxynitrite

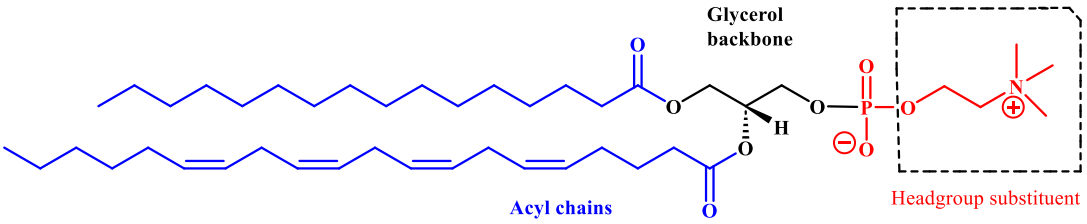
PA	Phosphatidic acid
pbf	2,2,4,6,7-pentamethyldihydrobenzofuran-5-sulfonyl
PC	Phosphatidylcholines
PE	Phosphatidylethanolamine
PEG	Polyethylene glycol
PG	Phosphatidylglycerol
PI	Phosphatidylinositol
PS	Phosphatidylserine
RBF	Round bottom flask
RES	Reticuloendothelial system
R_f	Retention factor
RGD	Arginine-glycine-aspartic acid
RO	Alkoxy
ROOH	Organic peroxides
ROS	Reactive oxygen species
SUV	Small unilamellar vesicles
T3P	propylphosphonic anhydride
TEA	Triethylamine
TEG	Tetraethylene glycol
TFA	Trifluoroacetic acid
THF	Tetrahydrofuran
T_m	Melting Temperature
UV	Ultraviiolet

Chapter 1. Background

1.1 Introduction to Liposomes

Liposomes are spherical lipid bilayer vesicles that typically have a diameter between 50 and 500 nm.[1] These vesicles are formed by self-assembling diacyl-chain phospholipids in an aqueous solution, creating a lipid bilayer. Lipid structure is commonly comprised of a hydrophilic phosphate head linked to hydrophobic tails by a water-soluble molecule like glycerol, which can either be natural or synthetic.[2, 3] The hydrophilic heads can be negatively charged, positive charged, or zwitterionic (containing both charges in the same molecule). These head group charges are crucial for the diverse functionality of liposomes in biological systems. Depending on the head groups, the family of phospholipids comprises (Figure 1.1) phosphatidylcholines (PC), zwitterionic lipids with a choline headgroup, and provide a significant component of animal membranes.[4, 5] Other classifications of phospholipids are phosphatidylserine (PS) and phosphatidylinositol (PI), which are anionic lipids that interact with the positively charged regions of the peripheral and integral membrane proteins.[5] Other important phospholipids include phosphatidylethanolamine (PE), phosphatidylglycerol (PG), and phosphatidic acid (PA), each having an ethanolamine, glycerol, and phosphate head group, respectively.

Liposome diversity stems from varying lipid compositions, surface charge, and size. The classification of liposomes is commonly based on size and lamellarity (Figure 1.2). Unilamellar liposomes consist of three types of vesicles: small unilamellar vesicles (SUVs) with 20-100 nm diameters, large unilamellar vesicles (LUVs) with 100-1000 nm diameters, and giant unilamellar vesicles (GUVs) with diameters greater than 1000 nm .[3, 4] On the other hand, multilamellar vesicles (MLVs) and multivesicular vesicles (MVVs) have numerous layers and sizes larger than 500 nm.[5] Unilamellar liposomes are single-layered spherical vesicles containing an aqueous core, while multilamellar liposomes have a concentric, onion-like structure.[1, 3, 6] The multilamellar vesicles are formed from the aggregation of smaller unilamellar vesicles, creating layers of phospholipids separated by water.[6] The size of these vesicles and the number of phospholipid layers significantly influence their circulation time within the body and their ability to encapsulate drugs.[7] A key factor influencing liposome stability and size for drug delivery is the temperature at which the lipid structure transitions from a rigid to a fluid state.



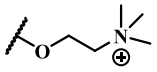
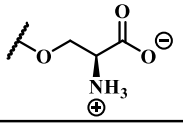
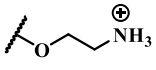
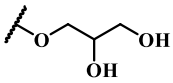
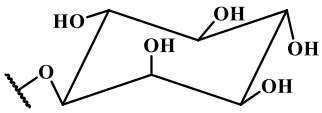
Glycerophospholipids types	Headgroup substituent	Headgroup structures
Phosphatidylcholine (PC)	Choline	
Phosphatidylserine (PS)	Serine	
Phosphatidylethanolamine (PE)	Ethanolamine	
Phosphatidylglycerol (PG)	Glycerol	
Phosphatidylinositol (PI)	Inositol	

Figure 1.1: Essential components of glycerophospholipids structure Glycerophospholipids consist of fatty acyl chains, a glycerol backbone, and a headgroup substituent. The head group substituents of glycerophospholipids determine their classification: anionic lipids are PS, PIs and PG, and zwitterionic lipids are PC and PE, respectively.

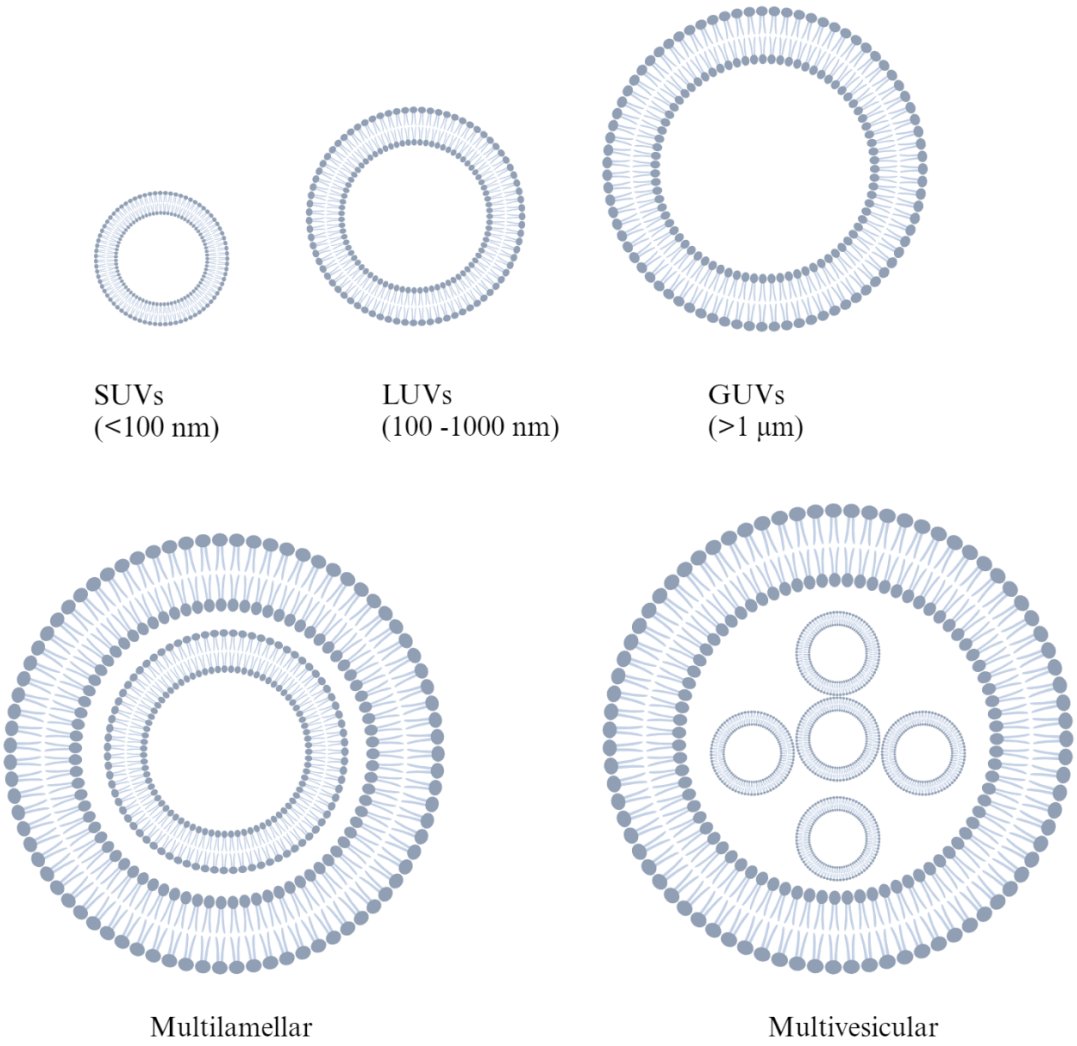


Figure 1.2: Liposomes classification according to their lamellarity and size. The sizes of large unilamellar vesicles (LUVs) range from 100 to 1000 nm, whereas those of small unilamellar vesicles (SUVs) are less than 100 nm. Conversely, GUVs are bigger than 1 µm. Multilamellar vesicles include many layers of membrane, whereas multivesicular vesicles encase smaller vesicles. Image created with Biorender.

This critical temperature point, known as phase transition or melting temperature (T_m), is essential for optimizing liposome formulation.[5, 8] The T_m also impacts the arrangement and interaction of lipid molecules within a membrane. At higher T_m values, lipids pack more tightly due to stronger molecular interactions.[8] Conversely, lower T_m values result in looser packing and weaker intermolecular forces. Lipid fluidity is dependent on the surrounding temperature being higher than the T_m.[8, 9] Conversely, temperatures below T_m induce a rigid, gel-like state where lipid tails are tightly packed and extended. Both lipid states are essential for incorporating drugs into liposomes during formulation.

1.2 Liposomes in drug delivery

1.2.1 Overview of smart drug delivery systems

Traditional drug delivery methods include oral and injection routes, but these methods face challenges like nonspecific targeting, poor localization, limited solubility, and side effects.[7, 10] Innovative drug delivery systems known as smart nanocarriers have emerged to address these limitations. These nanocarriers are designed to encapsulate and transport drugs to specific target sites within the body, enhancing drug efficacy. Smart nanocarriers that have been developed include inorganic, polymeric, and biomimetic-based nanoparticles,[11] as illustrated in Figure 1.3. Each nanocarrier has distinct advantages, making it suitable for various therapeutic applications. Factors like drug type, target site, and desired pharmacokinetic profile[7, 11] should be carefully considered when selecting the most appropriate nanocarrier for drug delivery. This thesis will focus on liposomes, the most researched drug delivery systems.

1.2.2 Liposome-based drug delivery systems

Liposomes, recognized for their biocompatibility, are the most extensively studied drug delivery systems.[10, 13] Following their discovery in the 1960s, their potential as drug carriers was immediately apparent, leading to the development of various liposomal-based drugs.[1, 7] Many of these drugs are now approved or in clinical trials. In 1995, the first US Food and Drug Administration (FDA) liposomal drug - polyethylene glycol liposomal doxorubicin (DOX) - was approved and used to treat breast cancer.[14, 15] Beyond cancer treatment, liposomes have been used in numerous clinical trials to deliver anesthetic, antifungal, antibiotic, anti-inflammatory, and gene therapy drugs.[13] The Amphipathic nature of liposomes makes it easy for them to deliver both hydrophilic and hydrophobic drugs, solving the solubility issues of many

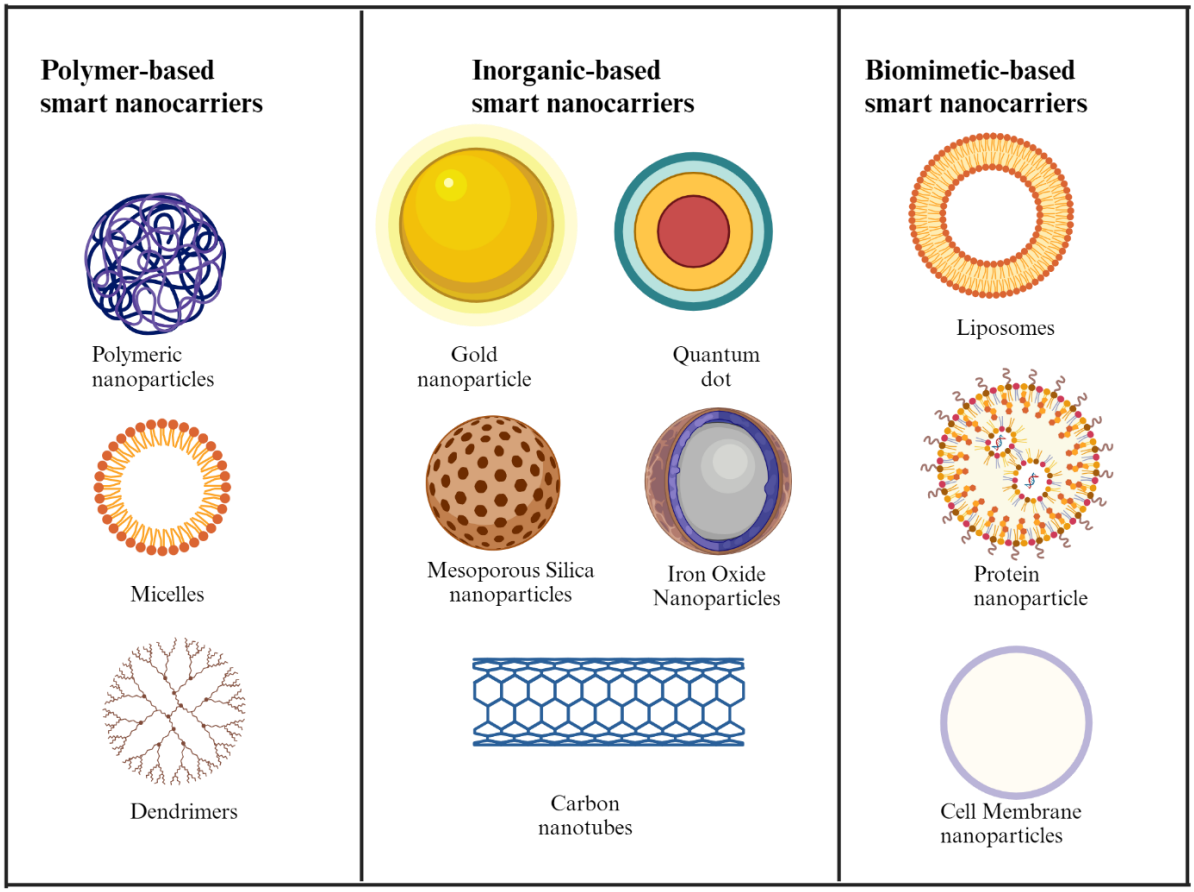


Figure 1.3: A visual representation of various smart nanocarrier types used for drug delivery. There are three main types of smart nanocarriers: polymer, inorganic, and biomimetic. The preferred nanocarrier to use is dependent on the drug type, intended site of action, and pharmacokinetic properties. This figure was generated using Biorender.com and is inspired by the work reported by **Cai et al.**[12]

drugs and leading to enhanced drug delivery with overall therapeutic outcomes. Liposomal delivery systems, with their particle size of approximately 100 nm, can avoid uptake by the reticuloendothelial system (RES), leading to enhanced pharmacokinetic properties.[9, 16] Factors like surface charge and the ability of these small liposomes to fuse with cell membranes also help improve liposomes' therapeutic potential.[16] Compared to traditional drug delivery methods, liposomal drugs often exhibit reduced toxicity and increased efficacy. While future liposomal applications are promising, their current use in the pharmaceutical industry establishes their importance in modern drug delivery systems.

1.2.3 Surface modifications of liposomes

Conventional liposomes (Figure 1.4A) have numerous advantages, such as biodegradability, biocompatibility, and the ability to encapsulate hydrophobic, hydrophilic, and amphiphilic compounds. While these merits have made liposomes renowned in drug delivery systems, some significant drawbacks of conventional liposomes include increased RES clearance, drug toxicity, and rapid clearance of liposomes from the bloodstream.[17] To overcome these limitations, surface modification has proven to be a successful strategy to reduce RES clearance, decrease drug toxicity, and improve the stability and half-life of liposomes in the bloodstream.[17] Liposomes coated with a hydrophilic polymer called polyethylene glycol (PEG) have been developed to enhance liposome stability and circulation time. Liposomes coated with PEG are also known as stealth liposomes because they are difficult for phagocytes to detect.[15] The PEG coating (Figure 1.4B) creates a steric barrier, preventing liposome aggregation and uptake by the RES.[18] The stealth property helps extend liposome circulation time from minutes to hours. Longer circulation time will allow the accumulation of liposomes at the tumor site more effectively by improving the liposome's enhanced permeation and retention effect. Also, PEGlated liposomes have a high degree of storage and lower aggregation rates in the bloodstream, increasing liposome bioavailability. While PEG remains the standard for the protection of liposomes to improve their circulation time and bioavailability, other polymers like L-amino-acid-based biodegradable polymer-lipid conjugates,[19] and 2-methacryloyloxyethyl phosphorylcholine[20] have been used for the coating of liposomes.

In addition to using PEG to modify the surface of liposomes, targeted ligands (Figure 1.4C) such as antibodies, carbohydrates, and peptides have been directly attached to the surface of

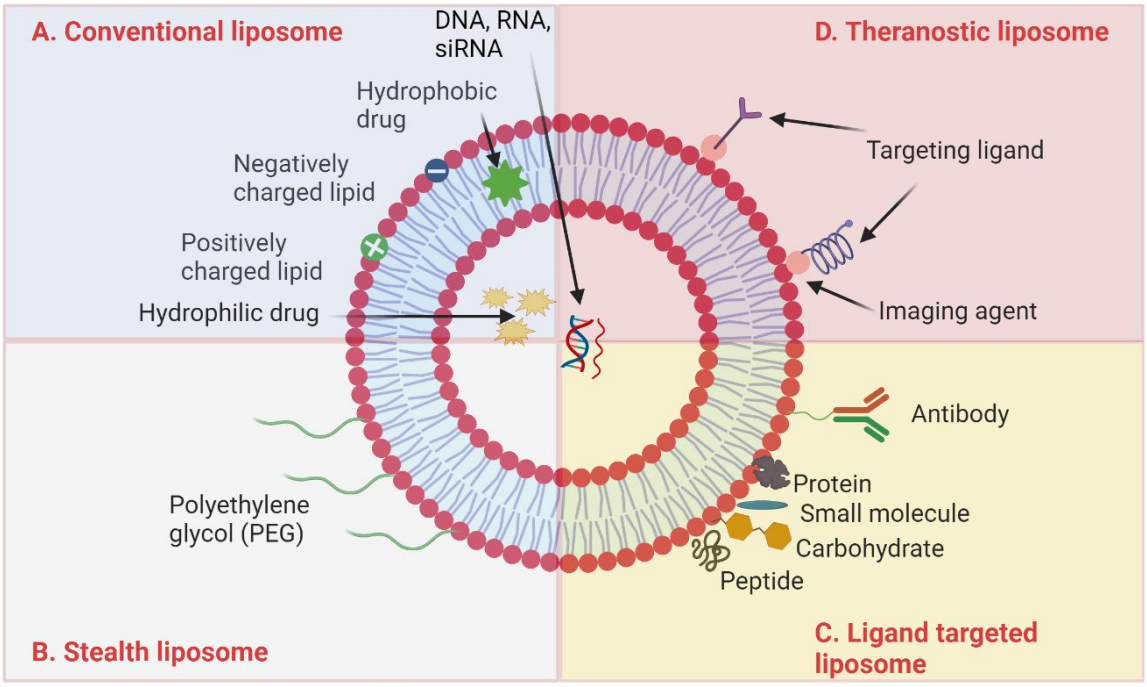


Figure 1.4: Cartoon depicting various types of liposomes and their functional modification. **(A)** Conventional liposomes are composed of lipids that can be neutral, positively charged, or negatively charged. **(B)** Stealth liposomes are coated with PEG polymers to increase their lifespan in the body. **(C)** Ligand-targeted liposomes are decorated with small molecules, antibodies, or peptides to precisely target specific cells or tissues. **(D)** Theranostic liposomes combine imaging agents and targeting molecules for diagnostic and therapeutic applications. This figure was created using Biorender.com and is inspired by the work reported by **Hue et al.**[23]

liposomes or to the end of PEG chains to improve liposomal drug accumulation in the desired organs or tissues. These ligands bind to specific receptors overexpressed on diseased cells, directing the liposome-encapsulated drug to the target. One of the most common ligands used in modifying liposomal bilayers is hyaluronic acid (HA), a ligand for various receptors such as CD44[21] and the lymphatic vessel endothelial HA receptor that are overexpressed in many cancer cells.[22] Various chemical methods, such as attachment to the carboxylate group on glucuronic acid, the primary hydroxyl on N-acetylglucosamine, or via reductive amination can be used to achieve this modification of liposomal bilayer with HA. Liposomes conjugated with HA-phosphatidylethanolamine have been used to target CD44 receptors, achieving multipoint attachment of HA to the liposome surface.[21]

Another versatile strategy used in liposomal surface modification is using antibodies to create antibody-coupled liposomes (immunoliposomes).[24] Antibody molecular structure consists of functional groups like sulfhydryl, carbohydrates, and amines. These functional groups are proper targets for antibody conjugation during the formation of antibody-targeted liposomes, which are formed by replacing the terminal methoxy group of PEGylated liposomes with the functional groups.[17] One of the molecules used in forming antibody-targeted liposomes is 2-iminothiolane, a molecule used for antibody thiolation.[25] The mechanism involved in antibody thiolation consists of the reaction of 2-Iminothiolane with primary amines in antibodies to form free sulfhydryl groups. These sulfhydryl groups can then be used to attach antibody fragments to liposome surfaces via a thioether bond. Various antibody fragments, such as anti-epidermal growth factor receptor,[26] and fragment antigen-binding anti-human epidermal growth factor-2 tyrosine kinase receptor,[21] have been successfully attached to liposomes. Additional molecules such as poly(ethylene glycol)-distearoylphosphatidylethanolamine-maleimide[20] and dipalmitoyl-L-cY- phosphatidylethanolamine[24] have also been used to attach antibodies to liposomes. In addition to antibodies, other liposomes surface modification moieties include aptamers[27] which have more affinity and selectivity for their designed antigen, peptides such as arginine-glycine-aspartic acid (RGD) peptide or cell-penetrating peptides,[28] small molecules, etc. Recent advancements in pharmaceutics have led to the development of theranostic liposomes, which integrate both imaging agents and therapeutic or targeting agents into a single delivery system (Figure 1.4D).

1.3 Integrins

Integrins are transmembrane receptors that play a crucial role in cell adhesion. They act as linkers between the extracellular matrix (ECM) and the cytoskeleton,[29] allowing for the transmission of biochemical and mechanical signals between cells and their environment. Mammalian integrins have two components: an alpha subunit and a beta subunit.[30] These components work together to form a receptor located on the cellular surface. There are 18 distinct α-subunits and 8 distinct β-subunits, which can combine in various manners to create 24 unique heterodimeric transmembrane receptors.[30] Among the 24 known integrin heterodimers,[31] αvβ3, αvβ5, and α5β1 are the most studied due to their increased expression on specific cancer modulate complex signaling processes in the cells, including cell migration, embryogenesis, cells and blood vessels that facilitate the growth and spread of tumors.[32, 33] Integrins processes can occur in two directions: "inside-out" or "outside-in." During "inside-out signaling" (Fig 1.5) an intracellular activator binds to the β-subunit of the integrin,[30, 35] changing its shape and making it more likely to bind to an extracellular ligand. This process is shown to facilitate the regulation of cellular adhesion, migration, and dissemination. During "outside-in-signaling" (Figure 1.5) a ligand binds to the integrin,[30, 34] which can cause multiple integrins to cluster together. This process initiates a sequence of events within the cell, resulting in changes in gene expression, cytoskeleton, and regulation of cell polarity and migration.[36] When integrins are not attached to any molecules, they can activate a protein known as caspase-8.[37] This protein can potentially induce cell death through a process referred to as "integrin-mediated death."(IMD)[32, 37]

1.3.1 RGD peptides and role in cellular targeting

Pierschbacher and Ruoslahti, in the early 1980s,[38] made a significant discovery when they identified that the RGD sequence, a short synthetic piece of the extracellular matrix fibronectin, could mimic the cell-attachment properties of the full-length protein.[39] Further research has revealed that the RGD peptide facilitates interactions between cells and their surrounding environment by binding to integrin receptors.[40] Among the integrin receptors, αvβ3 and αIIbβ3 are overexpressed on cancer cells and platelets, respectively.[35] The αvβ3 receptor, abundantly expressed on specific cancer cells and activated endothelial cells within tumor blood vessels, is a promising target for delivering therapeutic or diagnostic agents directly to cancer cells.[32] RGD is widely used in designing targeted therapies, such as in drug-loaded nanoparticles and

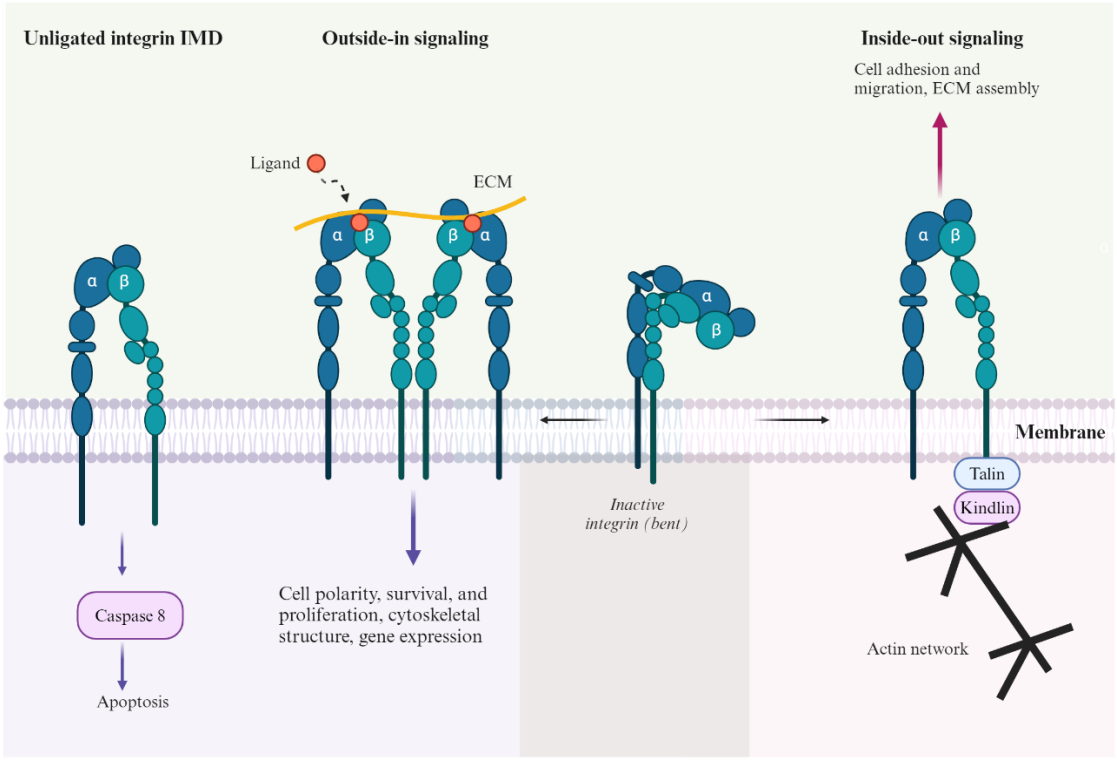


Figure 1.5: A diagrammatic representation of different states of integrin activation. This figure was created using Biorender.com and is inspired by the work reported by **Cheresh et al.**[32]

imaging agents for selective delivery to integrin-expressing cells, especially in cancer treatments.[41]

Numerous studies have explored the incorporation of RGD into liposomes and other nanoparticles for targeted delivery.[41-47] For instance, Amin et al. developed innovative cyclic RGD-modified liposomal delivery system to enhance tumor targeting while reducing off-target effects.[48] They designed many RGD peptides, including an N-methylated variant (RGDf[N-met]C),[48] to improve selectivity for αvβ3 integrins, which are frequently overexpressed in tumor cells and vasculature. In vitro and in vivo evaluations demonstrated that the RGD-modified liposomes exhibited enhanced targeting efficacy, reduced RES uptake, and increased tumor localization. Also, Zhang and co-workers developed RGD-modified liposomes that co-encapsulate combretastatin A-4,[49] a vascular disrupting agent, and doxorubicin, a cytotoxic drug, to improve tumor-targeted therapy. The study showed that RGD-modified liposomes exhibited increased intracellular absorption by tumor cells and human endothelium cells, in contrast to non-targeted liposomes. In vitro experiments demonstrated that RGD-modified liposomes showed increased cytotoxicity relative to non-modified liposomes, evidenced by a reduced IC_{50} (half-maximal inhibitory value).[49] The combination of these agents provided a synergistic therapeutic effect, making the RGD-modified liposomes a promising platform for improving cancer therapy through targeted administration of vascular disrupting and cytotoxic agents.

1.4 Reactive oxygen species (ROS) in drug delivery

1.4.1 Introduction to ROS

ROS are essential component in metabolic processes, and they help in the control of crucial physiological functions.[50] Examples include free radicals such as hydroxyl ($^{\bullet}OH$), superoxide ($O_2^{\bullet-}$), singlet oxygen ($^1O_2$), alkoxyl ($RO^{\bullet}$), peroxyl ($RO_2^{\bullet}$) and nonradicals such as peroxynitrite ($ONOO^-$), hypochlorite (OCl^-), hydrogen peroxide (H_2O_2), hypobromous acid (HOBr), organic peroxides (ROOH), ozone (O_3), and so on.[50, 51] The body typically sustains a fragile equilibrium between generating and eliminating ROS,[51] ensuring their concentrations remain minimal. Nonetheless, when this equilibrium is disturbed, the formation of ROS may escalate, resulting in numerous pathological diseases, such as cancer and inflammation. In regions impacted by these conditions, including tumor cells and activated immune cells, ROS levels can be markedly elevated, reaching concentrations of up to 100 μM, in contrast to 20 nM levels observed in

healthy cells.[52] The variation in ROS concentration has motivated researchers to create materials that react to increased ROS levels. These materials can be directed towards inflammatory or neoplastic sites, delivering their payloads particularly in areas with elevated ROS levels.[53]

1.4.2 Sources of ROS Generation

Mitochondria, endoplasmic reticulum (ER), peroxisomes, microsomes, and NADPH oxidase (NOX) complexes are the principal producers of intracellular ROS (Figure 1.6).[54, 55] Mitochondria are the primary intrinsic generators of ROS, producing them via the mitochondrial electron transport chain. Elevating cytoplasmic calcium (Ca^{2+}) concentrations activates the electron transport chain, generating increased ROS.[56] Also, minimal quantities of oxygen are produced in the production of adenosine triphosphate and water by the mitochondrion, triggering the generation of ROS. The initial ROS formed by mitochondria is the superoxide anion,[54] produced by complex I and complex III functions in the mitochondrial matrix and intermembrane space, respectively.[56] In the intermembrane gap, metal-containing enzymes, such as superoxide dismutase,[57] facilitate the transformation of superoxide anions into H_2O_2. Moreover, monoamine oxidase and α-ketoglutarate dehydrogenase represent additional potential mitochondrial ROS production sources.[55] Aside from the mitochondrion, the ER also plays a vital role in ROS generation. The endoplasmic reticulum lumen creates an optimal oxidizing environment for protein folding and disulfide bond formation, facilitated by a high oxidized to reduced glutathione ratio.[58]

Extracellular sources of ROS formation encompass ROS-inducing factors such as radiation, contaminants, and nanomaterials. Oxidative stress elicits defensive mechanisms in macrophages and neutrophils, aiding in the defense against microbial invasions, cancer, and environmental toxins. Free iron (Fe^{2+}) is integral to ROS-induced toxicity as it participates in the Fenton process,[59]generating extremely reactive hydroxyl radicals. Free iron is a crucial determinant of the toxicity linked to ROS production.

1.4.3 Mechanisms of nanoparticle-mediated ROS generation

The formation of ROS by nanoparticles (NPs) is affected by parameters including particle chemistry, size, surface area, and nanoparticle internalization. In terms of surface area, smaller NPs exhibit larger surface areas-to-mass ratios, resulting in increased reactive sites.[51] Additionally, chemical interactions increased significantly on small nanoparticles because of

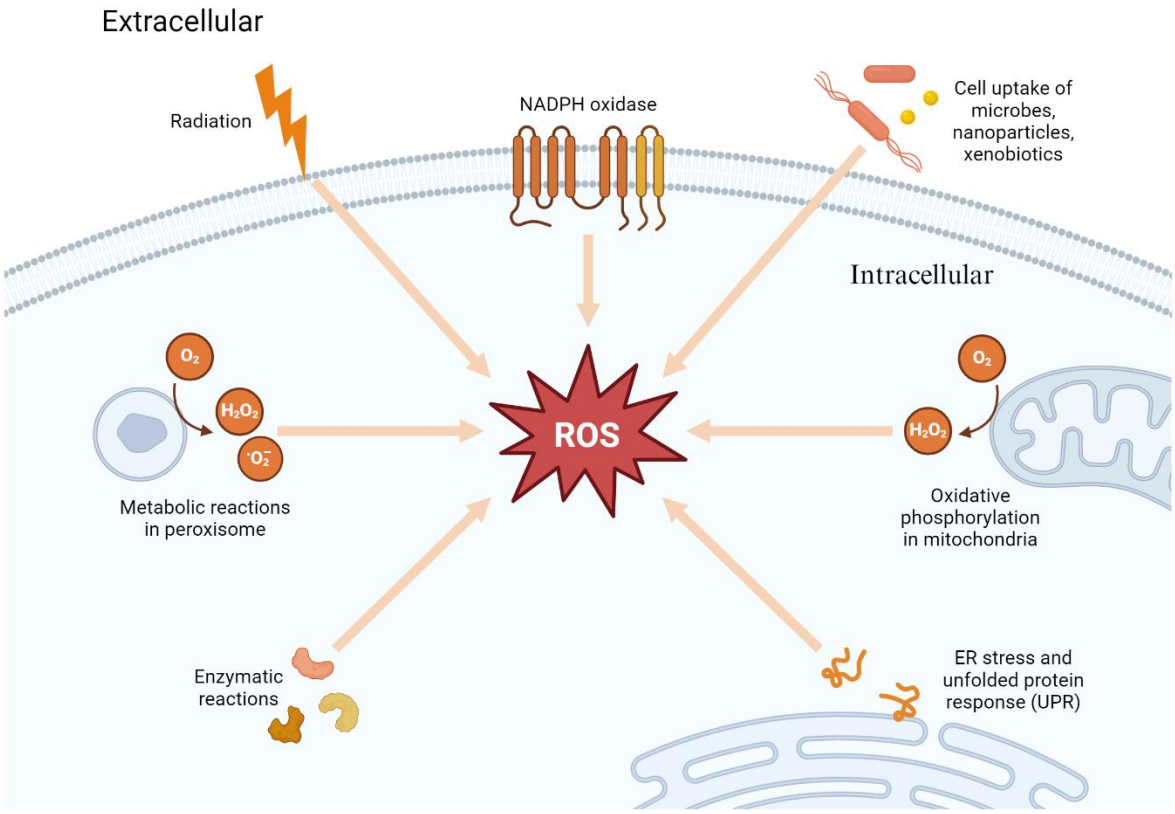


Figure 1.6: Schematic representation of the sources of ROS in biological system. The primary sources (intracellular) include mitochondrial electron transport, NADPH oxidase, peroxisomes, and enzymes. External factors like UV radiation and pollutants also contribute to ROS generation in cells. Image created with Biorender.com

their larger surface area. This high chemical reactivity stems from the surface atoms on the nanoparticles, which promote nanoparticle-mediated biochemical catalysis.[51, 59, 60] ROS production arises from free radicals and oxidants located on the NP surface. Research indicates that the generation of ROS, including $^{\bullet}OH$ and $O_2^{\bullet-}$ from quartz particles is attributed to the presence of surface-bound radicals, such as $SiO^{\bullet}$ and $SiO_2^{\bullet}$.[61]

The acceleration of ROS generation can also be affected depending on the presence of metallic elements or chemical compounds on the surface of the NPs. Transition metals like copper, silicon, iron, vanadium, and chromium facilitate the formation of ROS through the Fenton reaction mechanisms and the Haber-Weiss reactions.[51, 59] In the Fenton reaction, for example, the transition metal reacts with H_2O_2 to generate $^{\bullet}OH$ and an oxidized metal ion.[59, 61] Similarly, metallic NPs such as copper and iron affect oxidative stress ($^{\bullet}OH$ and $O_2^{\bullet-}$) through Fenton reactions, whereas the Haber-Weiss reaction entails the interaction of metal ions with H_2O_2,[62, 63] resulting in the generation $^{\bullet}OH$. Furthermore, NPs containing cobalt, chromium, and vanadium can catalyze both Fenton and Haber-Weiss reactions.[51]

1.4.4 ROS-responsive polymeric nanoparticles

Polymeric nanoparticles are formed through the self-assembly of amphiphilic block copolymers, and they serve as efficient carriers for the delivery of various imaging and therapeutic agents.[50] By carefully modifying the hydrophilic-lipophilic balance of the block copolymers[64] and the parameters governing their self-assembly, the physical characteristics, including shape and dimensions, can be effectively regulated, which will significantly impact the distribution within the body.[65] The incorporation of ROS-responsive polymeric nanoplatform has gained significant attention over the years. Some of the ROS-responsive units incorporated in polymeric nanoparticles includes: selenium, arylboronic esters, thioether, thioketal, tellurium etc. Researchers have been inspired to exploit the diselenide and monoselenide bond for development of stimuli-responsive drug delivery systems. For instance, Zhang and co-workers pioneered the use of diselenide bonds in the creation of ROS-responsive micelles.[66] They developed a triblock copolymer composed of PEG, polyurethane containing diselenide bonds and PEG (PEG-PUSeSe-PEG).[66] These polymers self-assembled into micelles in water and could release a model drug in response to both glutathione and H_2O_2 stimuli.[66] Xu and his team expanded upon the ROS-responsive properties of PEG-PUSeSe-PEG[67] micelles to create light-responsive drug

delivery systems. They incorporated porphyrins, a type of photosensitizer, into the core of the micelles. When exposed to red light, the photosensitizer generated $^1O_2$, which triggered the cleavage of the diselenide bonds.[67] This disruption of the micelles led to the release of the encapsulated drug, doxorubicin.

Arylboronic acid/ester groups have been employed as ROS-sensitive moieties in many applications, including a solubility switch method based on H_2O_2 oxidation. For instance, Broaders and co-workers altered the hydroxyl groups of the water-soluble polymer dextran by including aryl boronic ester groups to produce water-insoluble oxidation-sensitive dextran (Oxi-DEX).[68] The Oxi-DEX microparticles were subsequently fabricated via a double emulsion technique. The oxidation of boronic esters by H_2O_2 revealed the hydroxyl groups of dextran, resulting in the polymer's reversion to its hydrophilic parent form. This transition led to polymer breakdown and the liberation of contained payloads.[68]

1.5 Summary

Liposomes are popular nanocarriers due to their capacity to deliver hydrophilic and hydrophobic drugs, utilizing their hydrophilic core and lipid bilayers. However, a key limitation is their lack of specificity and the challenge of efficiently targeting diseased cells, often resulting in off-target effects. Another major hurdle is ensuring sufficient uptake of liposomes by diseased cells, which hinders the effectiveness of liposomal drug delivery. This thesis describes the design and synthesis of boronate-caged RGD-lipid, which ROS activates to enhance liposomal entry into cells.

Chapter 2. Enhanced Targeting of Cellular Delivery through ROS – Activated liposomes Utilizing a Boronate-Caged RGD Lipid

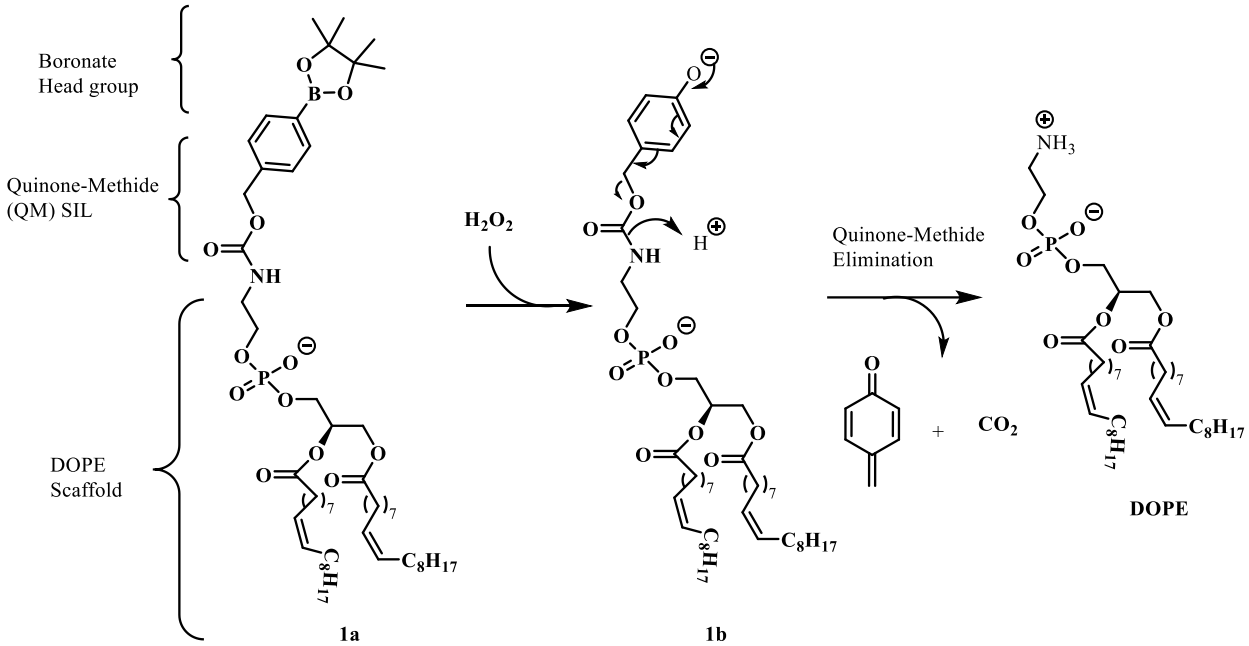
2.1 Overview and rationale of project

Liposomes are comprised of amphiphilic molecules, often phospholipids, that can spontaneously form lipid bilayers that can enclose an aqueous core.[69] Liposomes possess structural features that make them exceptionally adaptable for delivering a wide array of substances, including large-scale therapeutic agents like proteins, peptides, and nucleic acids, as well as chemotherapeutic drugs such as paclitaxel and doxorubicin, to diseased tissues and cells. Although liposomes have proven advantageous as drug delivery vesicles due to their extended circulation time, reduced toxicity, and enhanced pharmacokinetic properties,[7] the main drawback of liposomal drug delivery is their lack of selectivity and limited ability to target drugs specifically to diseased cells. Furthermore, the ability to achieve adequate internalization of liposomes by diseased cells continues to pose a substantial obstacle, hindering the overall efficacy of the liposomal drug delivery system.[70]

This project focuses on the design and synthesis of ROS-responsive RGD lipids to address the challenges of liposomal drug delivery, such as uncontrolled targeting and limited cellular uptake. The choice of RGD is deliberate, considering its established affinity to cell-surface receptors (integrins) that are highly expressed on cancerous cells.[71] The ROS-responsive RGD-modified liposomes are anticipated to interact with integrins, leading to the activation of intracellular signaling. This activation can potentially induce receptor-mediated endocytosis,[72] a critical process that facilitates the uptake of liposomes into cancer cells. Moreover, the specific nature of the interaction between the synthesized lipid and integrins guarantees that liposomes mostly focus on cells that have increased integrin expression, reducing unintended effects on non-target cells.[31] This characteristic enables a greater accumulation of therapeutic cargo sent to diseased tissues. Although considerable research has been conducted on liposomes that respond to ROS, combining the RGD moiety that targets integrins and the ROS stimuli associated with diseased cells can improve the selectivity and specificity of liposomes towards diseased cells. This will ensure therapeutic drugs are effectively delivered to the desired cellular locations, enhancing treatment outcomes.

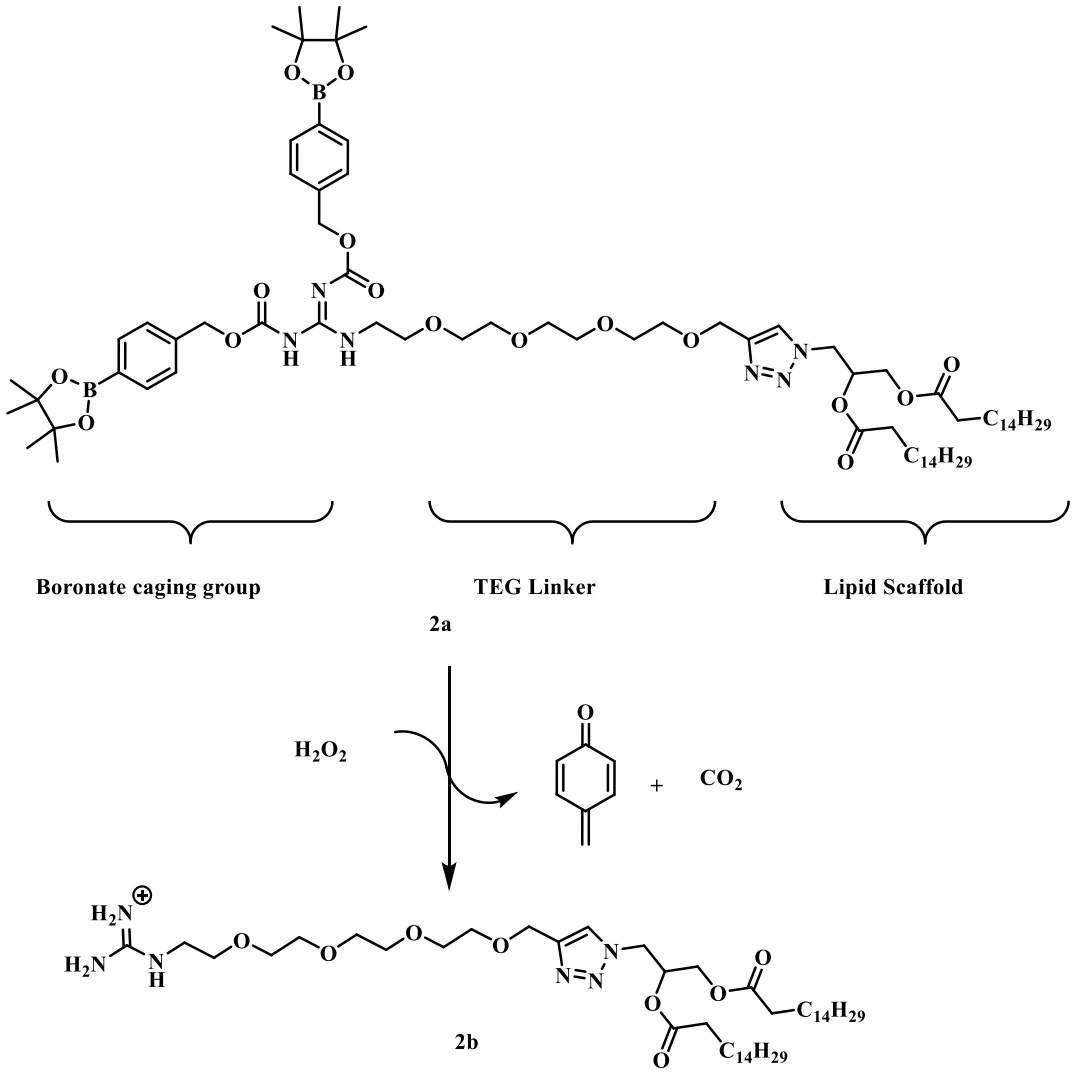
2.2 Previous Research on ROS-responsive liposomes

ROS-responsive liposomes have attracted significant interest due to their potential for selectively targeting disease sites with high ROS concentrations, such as fibrotic tissues, tumors, and inflammation. Although extensive research has been conducted on ROS-responsive nanocarriers, a very limited number of studies specifically focus on liposomes. Nevertheless, a few notable studies have shown the capabilities of ROS-responsive liposomes for precise drug delivery. Best's lab has made substantial contributions to the advancement of ROS-responsive liposomes. Best and coworkers developed a ROS-responsive liposomal platform using a synthetic lipid **1a** that enables the controlled release of cargo in environments rich in ROS. This lipid has a boronate ester headgroup that reacts with H_2O_2, a self-immolating linker that generates a quinone-methide, and a lipid scaffold called dioleoylphosphatidylethanolamine (DOPE)[73] (scheme 1). The study showed that the oxidative cleavage of the boronate ester headgroup by H_2O_2 is sufficient to induce the release of hydrophobic contents from the liposomes. However, for hydrophilic cargo release, generation of DOPE was required. The results showed that liposomes containing varying percentages of lipid **1a** exhibited dose-dependent release upon H_2O_2 addition.[73] Furthermore, the Best lab designed a novel ROS-responsive liposomal platform using a boronate caged guanidine lipid **2a** that H_2O_2 activates.[74] Upon activation, the boronate group is cleaved generating a cationic guanidine lipid **2b** (Scheme 2). Their results showed that liposomes containing lipid **2a** increased in positive charge after exposure to H_2O_2, indicating successful activation of the cationic guanidine lipid. The liposomes that were treated with higher concentration of H_2O_2 (0.5 - 1 mM)[74] showed greater changes in surface charge, confirming the ROS-responsive nature of the system. Using fluorescence microscopy, the study showed that ROS-activated liposomes significantly enhanced cellular uptake in cancer cells, but only after treatment with H_2O_2. Furthermore, Li and coworkers, for instance, developed ROS-sensitive liposomes based on a novel thioether phosphatidylcholines for drug release.[75] The functionalized liposomes were exposed to H_2O_2, and this caused the hydrophobic thioethers in the liposomes to undergo oxidation, resulting in the formation of hydrophilic sulfoxides or sulfones.[75] This process changed the characteristics of the liposome membrane and allowed for the release of hydrophilic drug such as doxorubicin, that were previously encapsulated. This approach showcased the effectiveness of ROS-responsive liposomes for drug release.



Scheme 1: Synthesis of ROS-responsive lipid 1a

Lipid **1a**, a ROS-sensitive lipid, possesses a boronate head that is susceptible to degradation by H_2O_2. Exposure to H_2O_2 results in the degradation of the boronate group, leading to the disintegration of the lipid structure. This releases DOPE, a lipid that can disrupt membrane integrity and trigger liberation of encapsulated cargo. [Adapted from reference[73]]

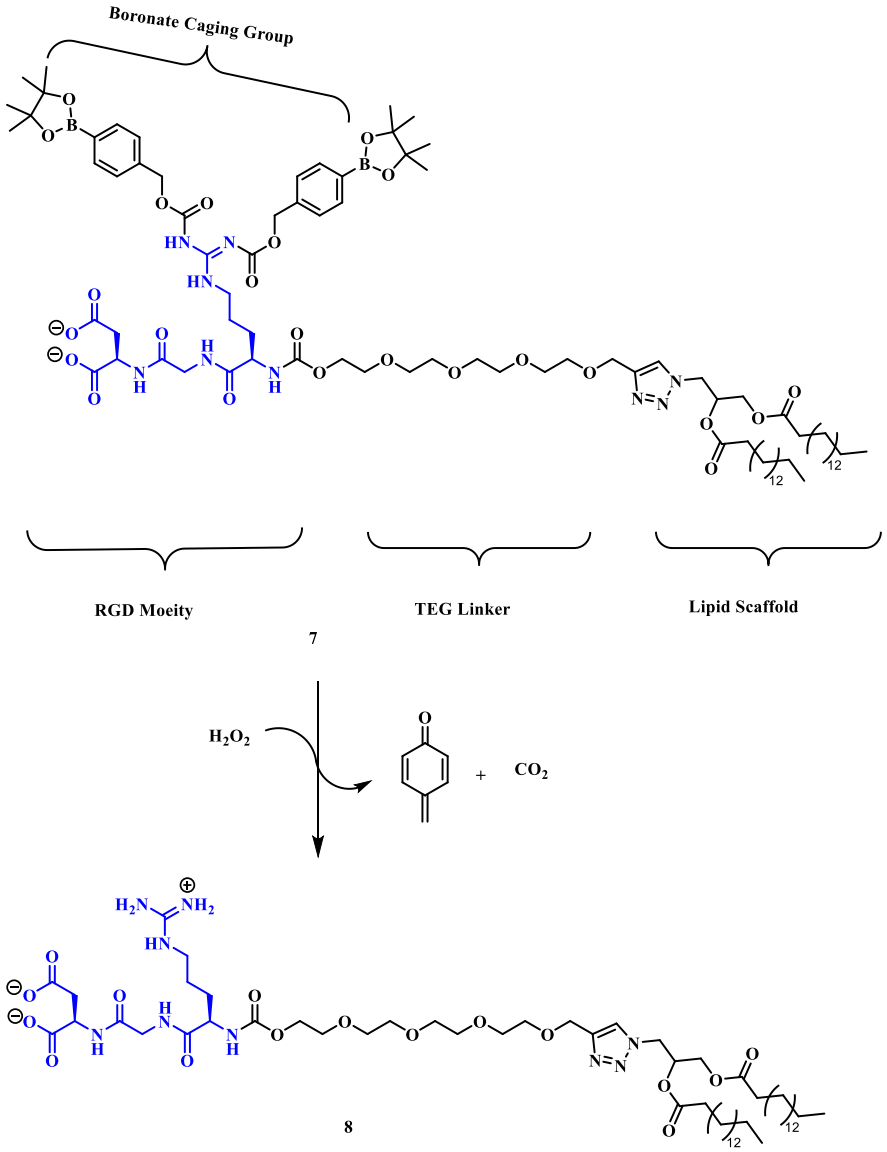


Scheme 2: Synthesis of a caged guanidine lipid 2a
Lipid **2a**, a caged guanidine lipid, possesses a boronate ester headgroup susceptible to degradation by H_2O_2. Upon exposure to H_2O_2, the boronate group undergoes cleavage to form cationic lipid 2b designed to enhance cell entry. [Adapted from reference [74]]

Also, Wang et al. synthesized ROS-responsive liposomes, referred to as DTP@DMF NPs,[76] with an ideal particle size, negative zeta potential, and effective release of DTP@DMF NPs in high levels of ROS. The liposomes demonstrated both efficient drug transport and decreased macrophage activity and fibrosis in mouse models, resulting in elevated ROS generation.[76] Further in vivo experiments provided additional evidence of the antifibrotic properties of DTP@DMF NPs, hence demonstrating their improved therapeutic effectiveness. With continued research and development, ROS-responsive liposomes hold significant potential for advancing therapeutic strategies in a range of diseases.

2.3 Design of ROS-responsive RGD lipid

Our design for ROS-responsive RGD lipid **7**, shown in scheme 3, consists of an RGD moiety connected to the lipid headgroup masked by two arylboronic ester groups. Additionally, lipid **7** includes a tetraethylene glycol linker and a lipid scaffold. The boronate ester groups indicated are well-known for their use in materials that demonstrate reactivity towards ROS, due to their rapid decomposition upon exposure to hydrogen peroxide (H_2O_2).[77] Lipid **7** is designed to undergo an oxidation reaction when it encounters H_2O_2 (Figure 2.1). This reaction involves the insertion of an oxygen atom into the carbon-boron bond, forming an intermediate phenoxide, which plays a crucial role in forming specific self-immolating linkers responsible for producing quinone methide.[52, 77] After the oxidative cleavage, the remaining molecule structure will undergo an elimination reaction, which will liberate RGD- lipid **8** after reacting with hydrogen peroxide. Hydrogen peroxide is known to be crucial for maintaining the health and functionality of cells in biological systems.[50] This reaction leads to the release of another lipid component, lipid **8**, which aids in the uptake of cells. Lipid **7** has a tetraethylene glycol linker, which helps to attach the caged RGD headgroup to the lipid structure. The linker is essential for preserving the headgroup's visibility on the membrane bilayer's surface.[74] This prevents the headgroup from being buried within the bilayer and keeps the reactive boronate at a distance from the membrane surface. Furthermore, the presence of a triazole group is highly significant in the composition of lipid **7** since it mimics the characteristics of a lipid headgroup. Due to its polar nature, the triazole molecule has a predilection for the aqueous interface rather than the hydrophobic membrane environment.[74] Its presence aids in facilitating the production of lipid using the copper-catalyzed azide-alkyne cycloaddition (CuAAC) process.[74, 78]



Scheme 3: A caged RGD-lipid 7 that cleaves in the presence of hydrogen peroxide
Lipid **7**, a caged RGD-lipid, contains a boronate ester headgroup that cleaves in the presence of H_2O_2, converting it to RGD-lipid **8**. The exposed RGD-lipid **8** selectively binds to integrin receptors on the cell surface, enhancing the compound's targeting efficiency. At physiological pH (~7.4), the carboxylic acid group is deprotonated, resulting in a negative charge, further contributing to its bioactivity.

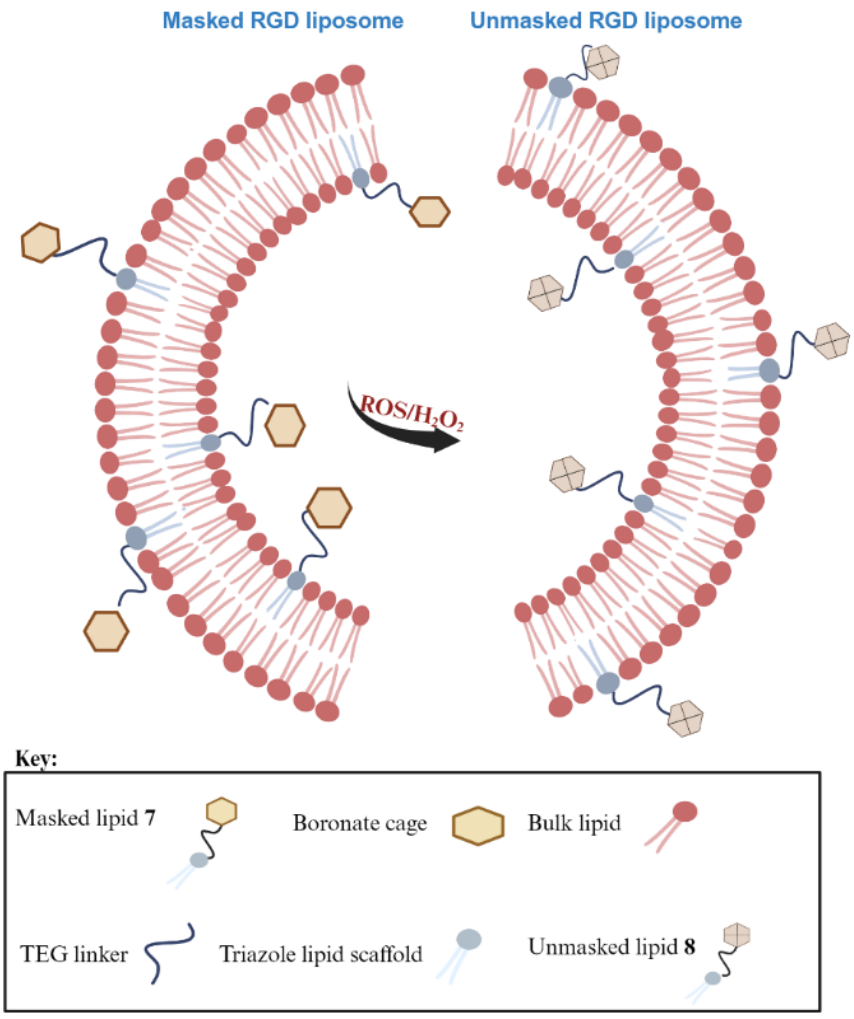


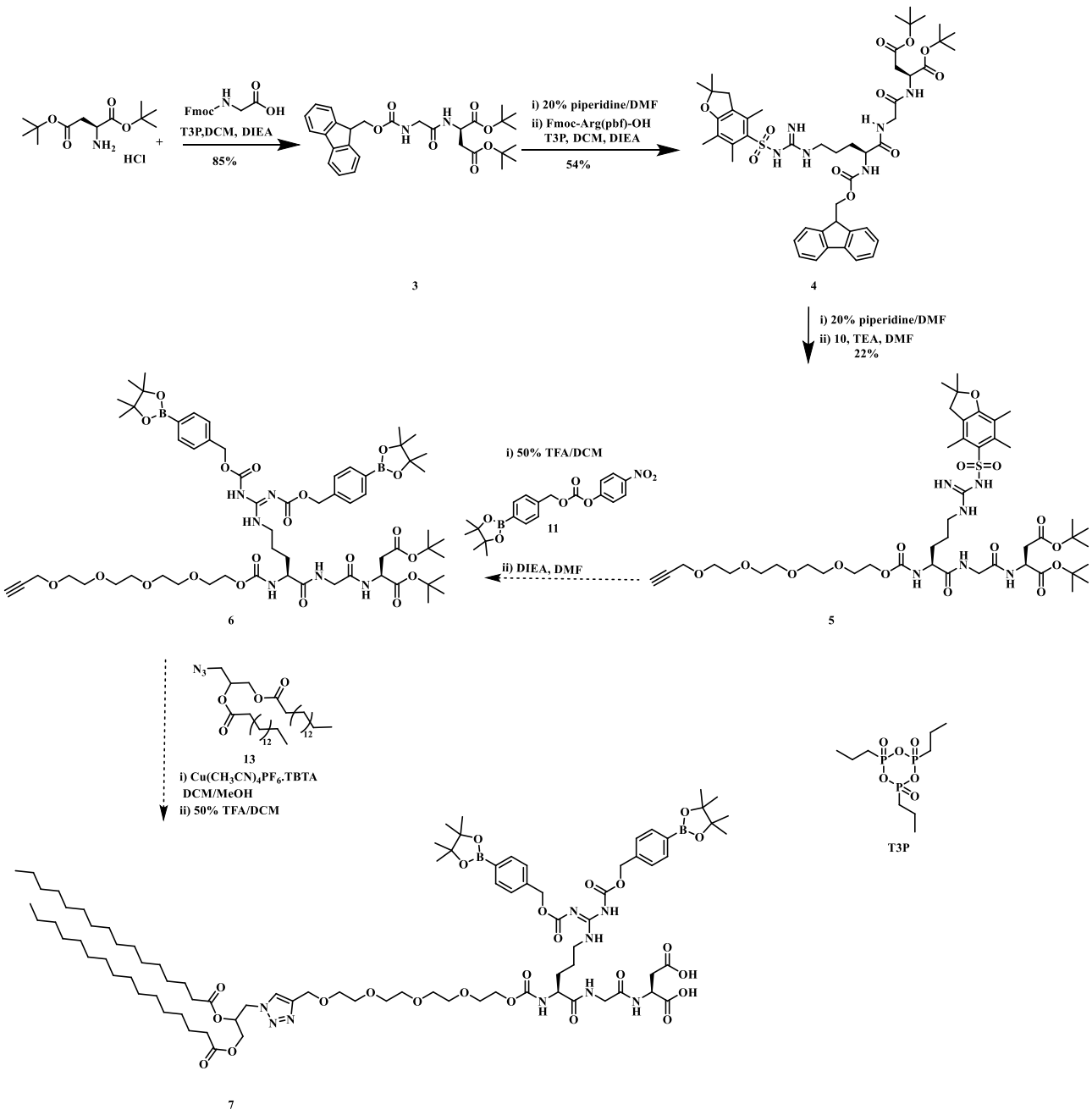
Figure 2.1: Cartoon showing boronate cleavage present in lipid 7 to form lipid 8
The cartoon shows the cleavage of boronate cage present in RGD lipid **7** to produce uncaged RGD lipid **8** that can improve cell targeting.

2.4 Synthesis Details of ROS-responsive RGD-lipid

The synthesis of ROS-responsive RGD-lipid **7**, as shown in Scheme 4, starts with an amide bond-forming coupling reaction. In the first step, the *N*-terminus, found in di-*tert*-butyl *L*-Aspartate hydrochloride (Asp (O*t*Bu)-O*t*Bu.HCl), was amide coupled to fluorenylmethoxylcarbonyl glycine (Fmoc-Gly) in the presence of *N*,*N*-Diisopropylethylamine (DIEA) - a base, and coupling reagent, propylphosphonic anhydride (T3P). T3P was used because it usually provides high yields, low racemization, and the ease of water removal of the ring opened by-product at the end of the reaction. The reaction was cooled in an ice-water bath to prevent racemization, which can occur at higher temperatures. Without additional purification, this resulted in compound **3**, in 85% yield after an aqueous work up. The proton NMR corroborated this by showing a doublet peak at 7.06 ppm, corresponding to the newly formed amide NH proton.

The next step involved the deprotection of the Fmoc group using a solution of 20% piperidine in DMF (*N*,*N*-dimethylformamide). The reaction was stirred for 4 hours to give a yellow solid, after which the solvent was removed. With no work-up, the resultant compound was then coupled to Nα-Fmoc-Nω-(2,2,4,6,7-pentamethyldihydrobenzofuran-5-sulfonyl)-*L*-arginine(Fmoc-Arg(pbf)-OH) via amide coupling to yield compound **4**, in 52% yield after silica column chromatographic purification. In the following step, the Fmoc group in **4** was removed, exposing the free amine at the *N*-terminus of the growing peptide chain. The deprotected amine from **4** attacks the already activated carboxyl group of **10**[74] leading to the formation of **5** in 22% yield. This nucleophilic acyl substitution forms a new amide bond that links the two molecules. The synthesis of **10**, a crucial connector in lipid **7**, entails a two-step procedure that will be explained in the subsequent paragraph.

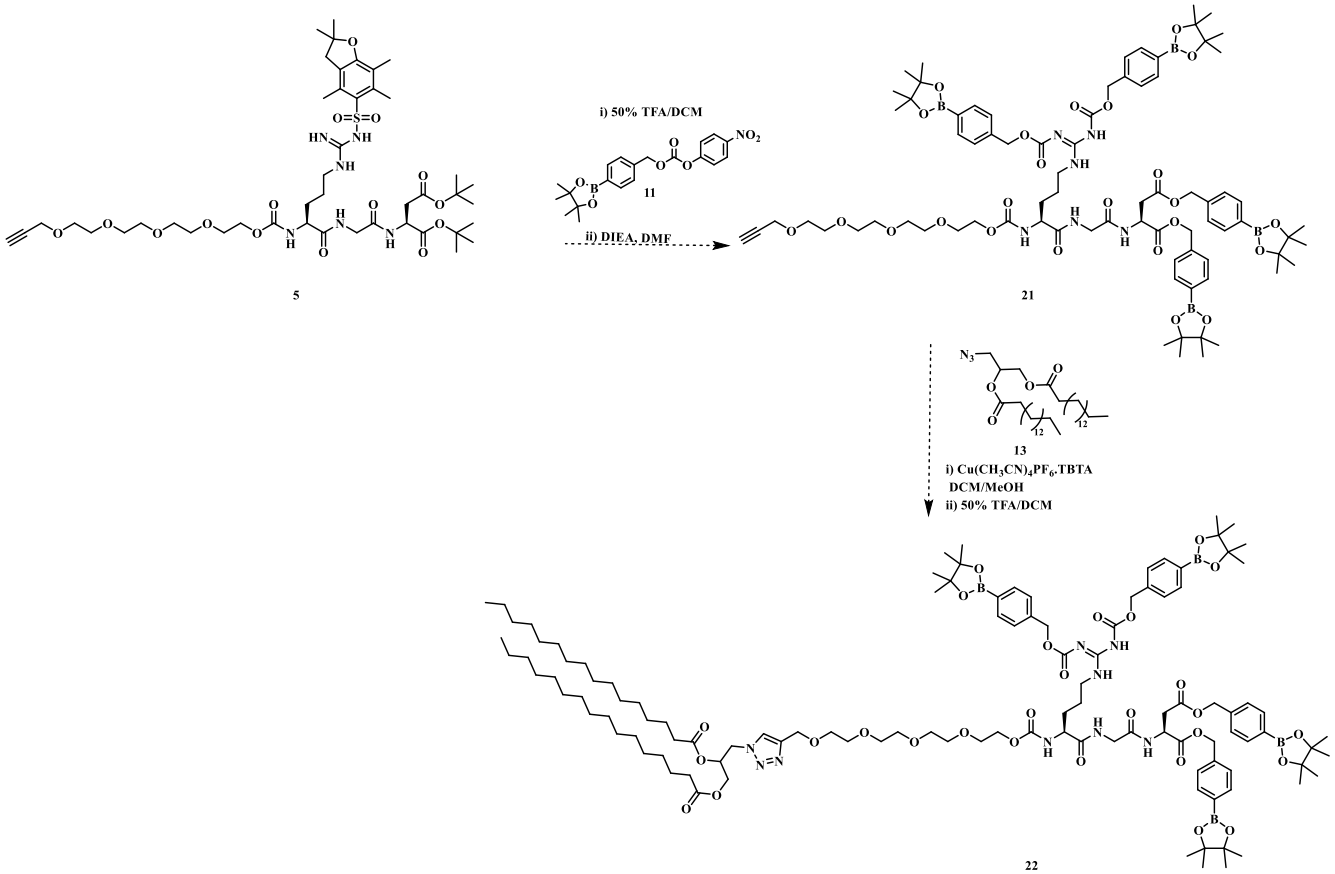
After synthesizing **5**, we attempted to deprotect the 2,2,4,6,7-pentamethyldihydrobenzofuran-5-sulfonyl (pbf) group attached to one of the terminal amine nitrogens on the guanidine group. The pbf group serves to prevent unwanted side reactions that might occur during the use of coupling reagents like T3P. However, during the deprotection process using trifluoroacetic acid (TFA), we observed that the TFA also affected the *tert*-butyl groups, which protected the carboxylic acid moieties at the C-terminus. Although this was an unintended side reaction, we proceeded with the reaction pathway to explore the possibility of grafting our boronate cage **11** onto the two



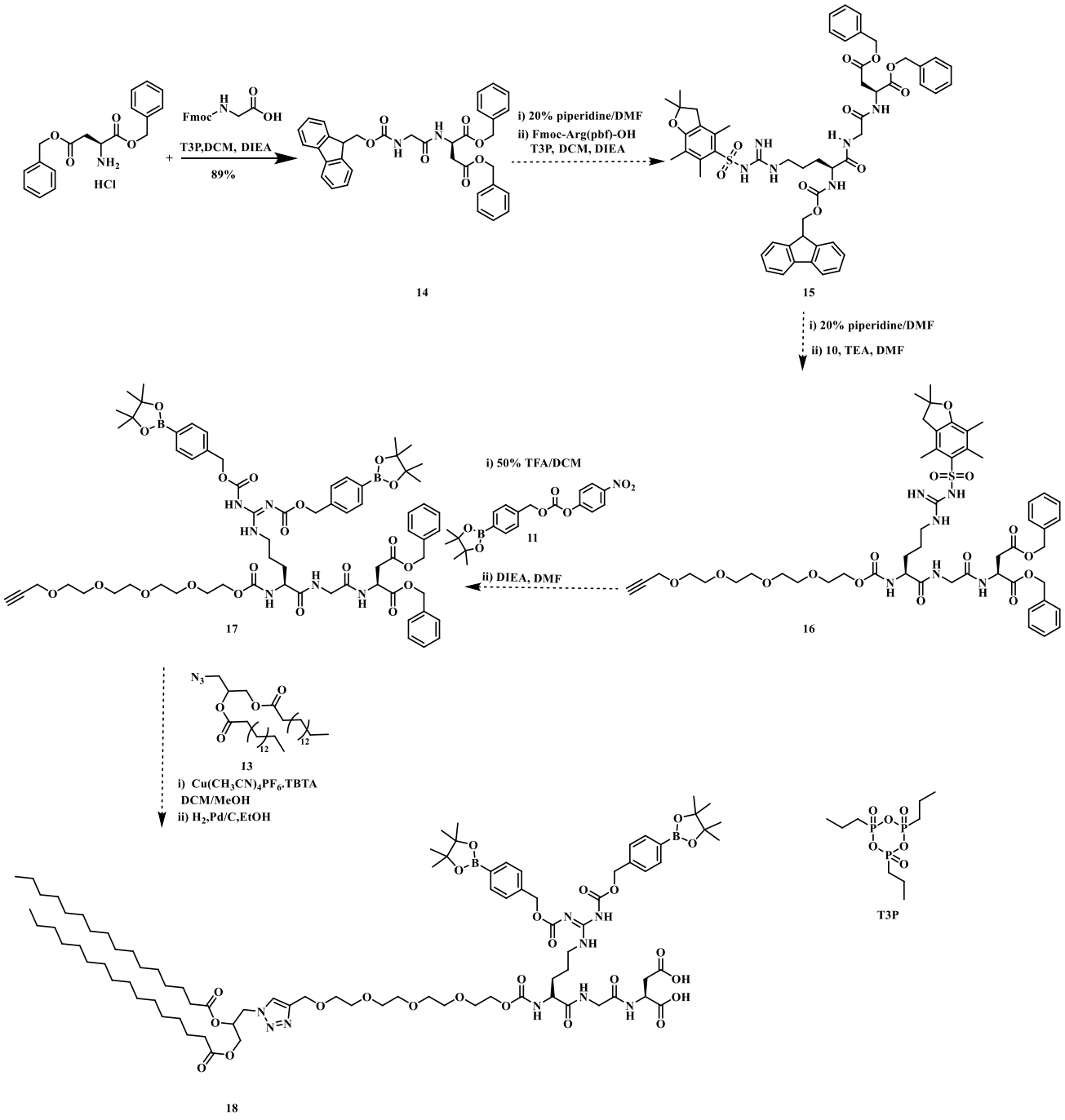
Scheme 4: Original synthetic route for lipid 7

guanidine nitrogens and the now unprotected carboxylic acid groups at the C-terminus (Scheme 5). Unfortunately, the reaction did not proceed as planned, as we encountered product degradation. This is probably because the reaction was carried out at elevated temperatures which resulted in the breakdown of the product. Analysis of the reaction mixture via NMR confirmed the presence of boronate cage alongside the fragments of the starting material. Although our initial goal was to synthesize a final compound in which the lipid **7** would retain an unprotected C-terminus, we believe this pathway is still worth exploring. We aim to conduct comparison testing between the resulting compound and the originally intended compound to assess their properties.

This problem made us rethink how best to graft the boronate cage onto the guanidine nitrogen without tampering with our desired structure. We began by designing a synthetic strategy that would enable the selective removal of the pbf protecting group using TFA, while ensuring the stability of the C-terminus of our compound. To achieve this, we employed a group that protects the terminal carboxylic acid, which is neither acid nor base-sensitive. Specifically, the benzyl group was chosen, as it can only be removed via hydrogenolysis, ensuring it remains intact under the TFA treatment used for pbf removal. This approach is supported by literature, where similar strategies are advantageous for reactions of this nature.[79] Our synthetic strategy would allow us to use trifluoroacetic acid to remove the pbf group without affecting the decomposition of the final product. In this revised strategy, *L*-Aspartic acid 1,4-bis-benzyl ester hydrochloride (Asp(OBzl)-OBzl.HCl) undergoes initial amide coupling with Fmoc-Gly to form compound **14** (Scheme 6). This approach closely follows our original synthetic route, with the primary difference being that the deprotection of the benzyl group will occur at the final stage of the reaction before coupling the resulting compound with the lipid tail **13**. While the first step of this new route has been completed with 89% yield, one challenge with the second step of the synthesis is solubility issues. It was not easy to get all our compound onto the column chromatography because it did not dissolve in dichloromethane. Although we thought the product was formed after confidently isolating the promising spot we observed from TLC (thin layer chromatography), the NMR results indicated some missing hydrogen signals, which we attributed to the incomplete recovery of the crude compound during the purification process. The synthesis of **10** involves initial mono-ether coupling of tetra ethylene glycol with propagyl

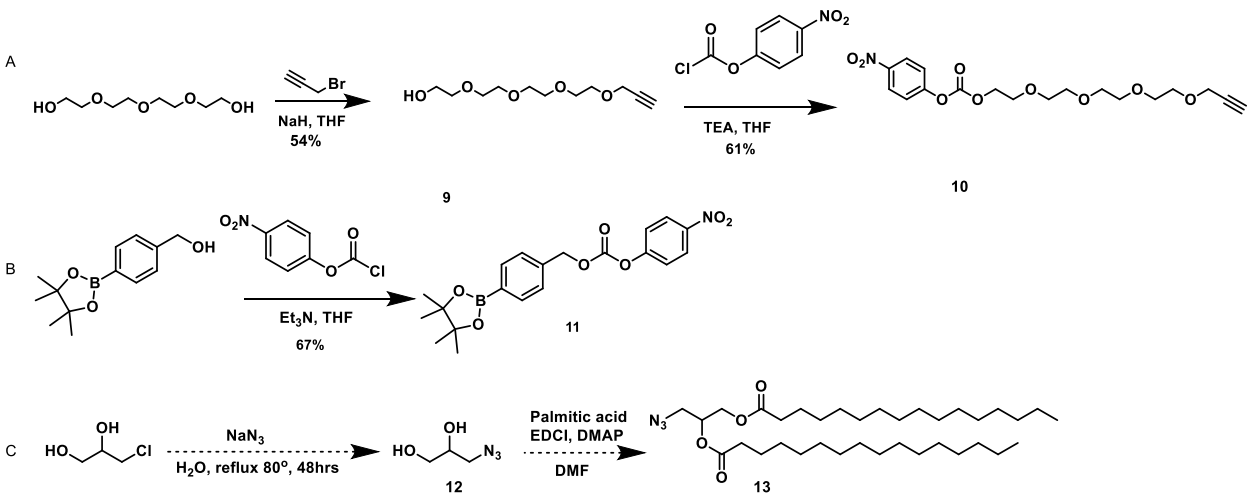


Scheme 5: Synthesis of caged terminal carboxylic acid, lipid 22

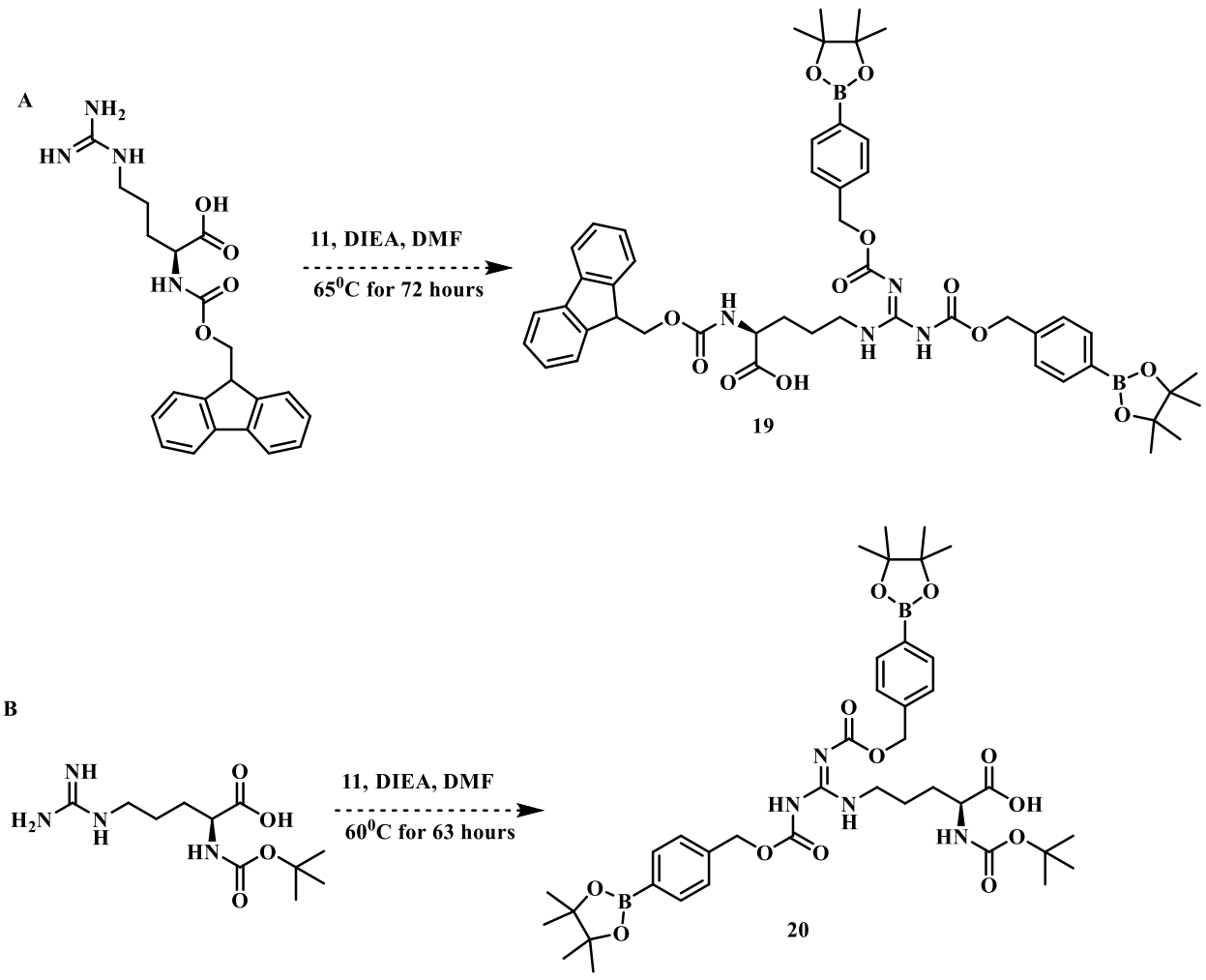


Scheme 6: Synthetic route for lipid 18

bromide to form **9.** Subsequently, the alcohol group in **9** was activated by using 4-nitrophenyl chloroformate to produce 4-nitrophenyl(3,6,9,12-tetraoxapentadec-14-yn-1-yl) carbonate (**10**) (Scheme 7A). The synthesis of arylboronate ester p-nitrophenol carbonate compound **11**, (Scheme 7B) was carried out by coupling 4-carboxyphenylboronic acid pinacol ester with 4-nitrophenyl chloroformate. In this reaction, the triethylamine (TEA) neutralizes the hydrochloric acid generated during the reaction and ensures the starting material is more nucleophilic by abstracting the hydroxyl group hydrogen. Upon nucleophilic attack by the phenoxide ion formed, the intermediate formed collapsed by releasing chloride ion. The chloride ion release helps create the desired ester bond between the phenolic oxygen and the acyl chloride carbonyl group. One of the challenges we have consistently encountered, even in our initial synthetic route, is grafting the boronate cage onto the guanidine nitrogens. To better understand this issue, we tested the reaction using a simpler model compound to assess whether the boronate group could be successfully grafted. We selected (2S)-5-(diaminomethylideneamino)-2-(9H-fluoren-9 ylmethoxycarbonylamino)pentanoic acid (Fmoc-Arg-OH) as our model compound (Scheme 8A). This choice was made because the two guanidine nitrogens in arginine are unprotected, making them accessible for potential grafting of the boronate cage. However, upon conducting the reaction, we identified a significant issue: the use of DIEA as a base at elevated temperatures posed a risk of deprotecting the Fmoc group. Unfortunately, elevated temperatures were necessary for the boronate caging process to proceed. After running the reaction at 65°C for 3 days, the NMR results initially appeared promising, but we observed the unintended removal of the Fmoc group due to the basicity of DIEA. We substituted DIEA with a weaker base, DMAP (4-dimethylaminopyridine) to address this. DMAP is a nucleophilic catalyst with a milder base than DIEA, making it less likely to remove the Fmoc group under similar conditions. The rationale behind using DMAP is that its basicity is sufficient to facilitate the boronate grafting reaction without causing side reactions, such as Fmoc deprotection.[78] Despite this adjustment, the desired product was still not obtained. Further optimization of reaction conditions, such as adjusting the temperature or reaction time, may be necessary to successfully graft the boronate cage onto the guanidine nitrogens without compromising the integrity of the Fmoc group. Aside from using Fmoc-Arg-OH, we also tested tert-butyl(tert-butoxycarbonyl)-*L*-arginate (Boc-Arg-OH.HCl) (Scheme 8B). This compound was used to avoid the potential removal of the Fmoc



Scheme 7: Synthetic route for the linker, boronate cage and lipid tail
A) Synthetic route for tetra ethylene glycol linker (**10**). B) Synthetic route for arylboronate ester (**11**). C) Synthetic route for the lipid tail (**13**)



Scheme 8: Synthetic trial of boronate caging of guanidine nitrogen on arginine
A) Synthetic trial of boronate caging of Fmoc-Arg-OH. B) Synthetic trial of the boronate caging of Boc-Arg-OH

group by DIEA. The Boc group, which protects the α-amino group of the arginine, was used because this group is acid labile, i.e., it can only be cleaved in the presence of acid. It is resistant to bases like DIEA, even at high temperatures. These features make it more stable under basic conditions, so we chose it. We carried out our reaction by coupling the boronate cage to the arginine guanidine nitrogens using DIEA as a base, and DMF as the solvent. After running the reaction for 63 hours at 60˚C, we removed the solvent. Because of the acid group in our compound, we decided not to perform an aqueous workup to avoid the compound dissolving into the aqueous layer, as carboxylic acids are water-soluble. We then performed column chromatography and took the NMR. The NMR result was promising as we saw two doublet peaks at 7.8 ppm, which are indicative of the boronate cage nitrogens. Although this pathway proved to be a valuable strategy for grafting the boronate cage onto the guanidine nitrogens, further optimization is still required to get accurate conditions for the reaction.

2.5 Conclusion

The main problem throughout our synthetic pathway has been the successful grafting of the boronate cage onto the guanidine nitrogens of arginine. Although our initial attempts were met with difficulties, the progression of this research has provided valuable insights into specific reaction conditions necessary for this critical step. The insights gained from these obstacles have resulted in a more profound comprehension of the complex equilibrium between preserving the integrity of the protective groups in our compound achieving efficient boronate caging. Future efforts will concentrate on refining reaction parameters and optimizing the last stages of our synthesis to guarantee the effective grafting of the boronate cage onto the guanidine nitrogens, while preserving the stability of other essential protective groups. Additionally, completing the synthetic pathway to achieve the final target compound would provide a comprehensive understanding of this ROS-activated system.

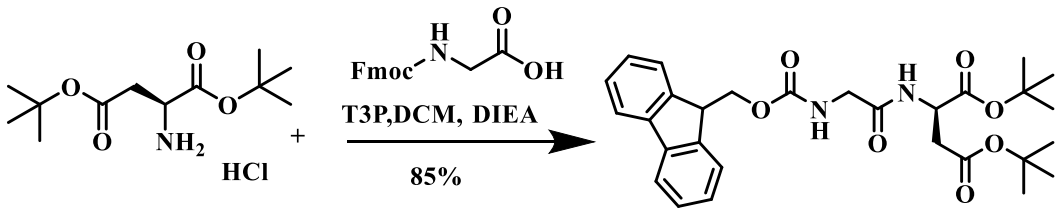
This work has made a significant contribution to the enhanced targeting of cellular delivery through ROS-activated liposomes with boronate-caged RGD lipid. The insights gained from the study not only provide a foundation for future optimization but also demonstrate the potential of boronate-caged RGD lipids in enhancing the specificity and efficacy of cellular delivery systems when the caged RGD-lipids is exposed to ROS.

2.6 Experimental

2.6.1 General Considerations

All reagents were procured from Aldrich and Ambeed, and they were utilized as received. Dry solvents were acquired from pure solvent delivery system from University of Tennessee. Column chromatography was carried out using 230 – 400 mesh silica gel purchased from sorbent technologies. NMR spectra were obtained using Varian VNMRS 500 MHz spectrometer and Bruker Avance NEO 500 MHz spectrometer.

2.6.2 Synthetic procedures



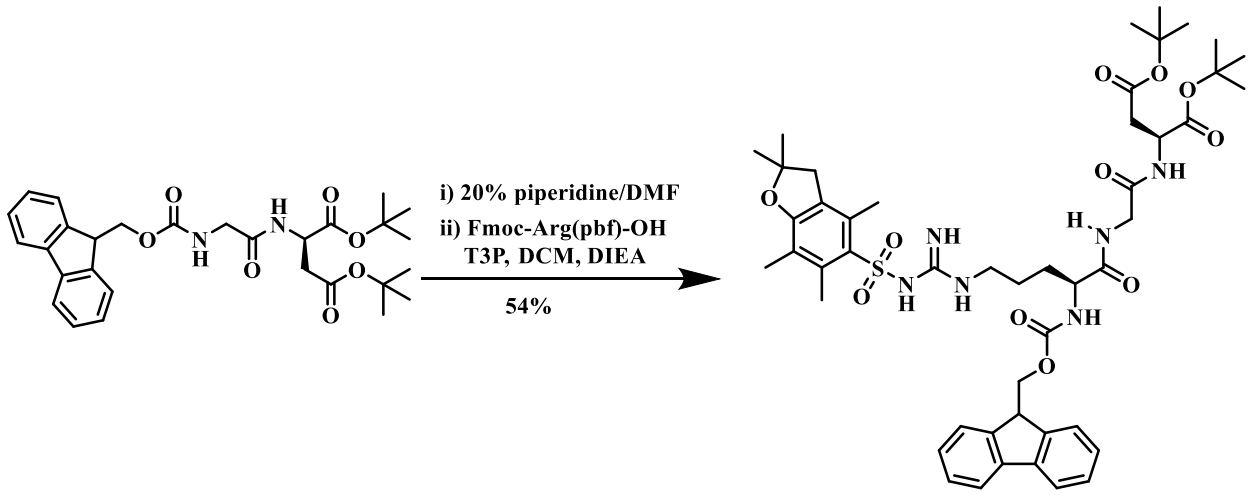
3

Synthesis of di-*tert*-butyl(((9H-fluoren-9-yl)methoxy)carbonyl)glycyl-D-aspartate (3)

In a 50 mL round-bottomed flask (RBF), di-*tert*-butyl L-Aspartate hydrochloride (0.14 g, 0.505, 1 eq) and fluorenylmethoxylcarbonyl glycine (0.15 g, 0.505 mmol, 1 eq) were dissolved with 10 mL of dry dicholoromethane under argon gas with stirring. Afterwards, N,N-Diisopropylethylamine (DIEA, 0.16 mL, 1.01 mmol, 2 eq) was added. The solution was cooled in an ice-water bath to 0°C and then propylphosphonic anhydride (T3P, 50 wt.% in ethyl acetate, 0.181 mL, 0.606 mmol, 1.2 eq) was added dropwise over 15 minutes. The ice-water bath was removed, and the reaction mixture was stirred for 24 h. The reaction mixture was then quenched with water (3 mL), and poured into a separatory funnel containing 5 mL water. The aqueous layer was extracted with 2 × 15 mL dichloromethane, and the combined organic layer was further washed with 15 mL of saturated sodium hydrogen carbonate ($NaHCO_3$), 1 × 15 mL water, and 1 × 15 mL brine. The organic layer was dried over sodium sulfate, filtered and concentrated under reduced pressure to produce the product **3** as a white foam (0.23 g, 85 % yield). No further purification was required. R_f = 0.67 (9:1 dichloromethane/methanol, UV and potassium permanganate stain). ^{1}H NMR (500 MHz, $CDCl_3$) δ 7.73 (d, *J* = 7.5 Hz, 2H), 7.59 (s, 2H), 7.36 (t, *J* = 7.5 Hz, 2H), 7.28 (d, *J* = 7.7 Hz, 2H), 7.06 (d, *J* = 8.2 Hz, 1H), 5.77 (d, *J* = 5.8 Hz, 1H), 4.72 (dt, *J* = 8.6, 4.5 Hz, 1H), 4.36 (d, *J* = 7.1 Hz, 2H), 4.20 (t, *J* = 7.2 Hz, 1H), 3.94 (t, *J* = 6.6

Hz, 2H), 2.87 (dd, *J* = 17.1, 4.5 Hz, 1H), 2.72 (d, *J* = 12.6 Hz, 1H), 1.43 (s, 9H), 1.40 (s, 9H). ^{13}C NMR (126 MHz, $CDCl_3$) δ 170.14, 169.55, 168.79, 156.53, 143.87, 143.84, 127.70, 127.09, 125.17, 119.95, 82.47, 81.63, 67.28, 49.16, 47.10, 44.36, 37.42, 28.02, 27.89.

NMR data matched that in the literature.[80]



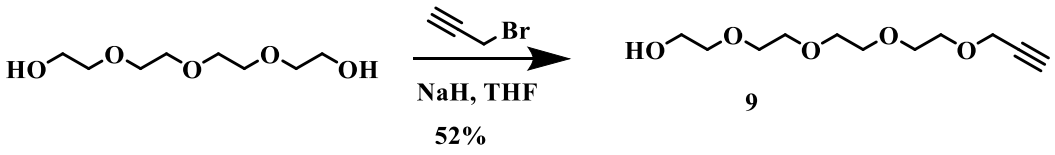
3 4

Synthesis of di-*tert*-butyl N^2-(((9H-flouren-9-yl)methoxy)carbonyl)-N^{ω}-((2,2,4,6,7-pentamethyl-2,3-dihydrobenzofuran-5-yl)sulfonyl-L-arginylglycyl-L-aspartate (4)

Compounds **3** (0.09 g, 0.172 mmol, 1 eq) was dissolved with 4 mL dimethylformamide in a 100 mL RBF under argon. After adding 0.8 mL piperidine, the reaction mixture was stirred at room temperature for 4 hours to yield a pale yellow solid. Next, the solvent was removed under reduced pressure and place under hivac for 2 hours to remove the residual solvent. Thereafter, Fmoc-Arg(pbf)-OH (0.11 g, 0.172 mmol, 1 eq) was added into the RBF under Argon, followed by addition of 6 mL of dry dicholoromethane and *N,N*-Diisopropylethylamine (DIEA, 0.056 mL, 0.344 mmol, 2 eq). The solution was cooled in an ice-water bath to 0°C and then propylphosphonic anhydride (T3P, 50 wt.% in ethyl acetate, 0.06 mL, 0.206 mmol, 1.2 eq) was added dropwise over 15 minutes. The ice-water bath was removed, and the reaction mixture was stirred for 24 hours. The reaction mixture was then quenched with water (3 mL) and poured into a separatory funnel containing 5 mL water. The aqueous layer was extracted with 2 × 15 mL

dichloromethane, and the combined organic layer was further washed with 15 mL of saturated sodium hydrogen carbonate ($NaHCO_3$), 1 × 15 mL water, and 1 × 15 mL brine. The organic layer was dried over sodium sulfate, filtered, and concentrated under reduced pressure. The crude was then subjected to silica gel column chromatography. Gradient elution from dichloromethane- 5% methanol-dichloromethane was used to obtain **4** as a white solid (0.0864 g, 54% yield). R_f = 0.3 (5% Methanol-Dichloromethane, UV and potassium permanganate stain). ^{1}H NMR (500 MHz, $CDCl_3$) δ 7.78 (s, 1H), 7.72 (d, *J* = 7.5 Hz, 2H), 7.60 – 7.53 (m, 2H), 7.35 (t, *J* = 7.5 Hz, 2H), 7.24 (d, *J* = 7.3 Hz, 2H), 7.20 (d, *J* = 8.3 Hz, 1H), 6.37 (s, 2H), 6.16 (d, *J* = 8.1 Hz, 2H), 4.67 – 4.62 (m, 1H), 4.42 – 4.29 (m, 3H), 4.15 (t, *J* = 7.3 Hz, 1H), 4.05 – 3.89 (m, 2H), 3.32 (s, 1H), 3.20 (s, 1H), 2.90 (s, 2H), 2.79 (dd, *J* = 17.1, 5.1 Hz, 1H), 2.66 (dd, *J* = 17.1, 4.7 Hz, 1H), 2.58 (s, 3H), 2.50 (s, 3H), 2.22 (s, 1H), 1.93 (s, 1H), 1.72 (s, 1H), 1.60 (s, 2H), 1.42 (s, 6H), 1.39 (s, 9H), 1.39 (s, 9H). ^{13}C NMR (126 MHz, $CDCl_3$) δ 173.06, 170.23, 169.85, 169.40, 158.84, 156.69, 156.59, 144.00, 143.88, 141.36, 138.50, 132.92, 132.42, 127.77, 127.19, 125.35, 124.70, 120.01, 117.60, 86.45, 82.73, 81.80, 67.18, 54.35, 49.50, 47.20, 43.33, 42.95, 37.42, 28.68, 28.13, 27.97, 25.26, 19.43, 18.09, 12.58.

NMR data matched that in the literature.[80]

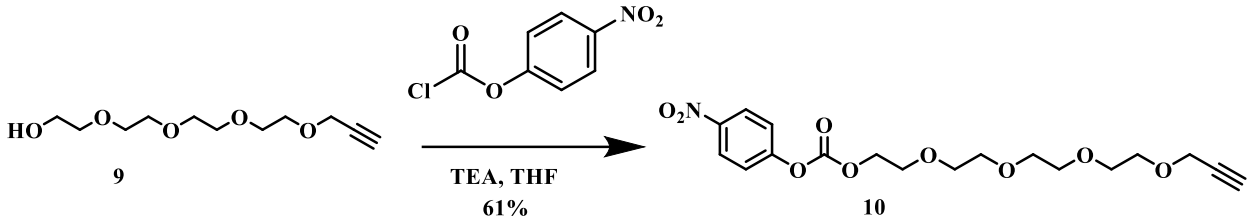


Synthesis of 3,6,9,12-tetraoxapentadec-14-yn-1-ol (9)

In a 200 mL RBF, 2,2'-((oxybis(ethane-2,1-diyl))bis(oxy)bis(ethan-1-ol) (0.971 g, 5 mmol, 2.5 eq) was dissolved with 20 mL dry tetrahydrofuran (THF) under argon. The reaction mixture was cooled in an ice-water bath to 0°C, and sodium hydride (NaH, 0.12 g, 5 mmol, 2.5 eq) was added. The solution was then stirred for one hour after which propagyl bromide (0.152 ml, 2 mmol, 1 eq) was added dropwise. The reaction mixture showed a color change from colorless to light brown and was stirred for 22 hours. Upon completion, the reaction was quenched by adding water dropwise, and the solvent was removed under reduced pressure. The residual was re-dissolved with 15 mL ethyl acetate and 15 mL of water and transferred into the separatory

funnel. The ethyl acetate layer was collected, and the aqueous layer was further extracted with 2 × 10 mL of ethyl acetate. The combined ethyl acetate layer was washed with 1× 50 mL of brine. After being dried over sodium sulfate, filtered, and concentrated under reduced pressure, the crude was subjected to silica gel column chromatography. Gradient elution from hexanes to 100% ethyl acetate was used to obtain the product as a colorless oil (0.25 g, 54 % yield). R_f = 0.2 (100% Ethyl acetate, potassium permanganate). ^{1}H NMR (500 MHz, $CDCl_3$) δ 4.09 (d, *J* = 2.6 Hz, 2H), 3.61 (d, *J* = 4.7 Hz, 2H), 3.59 (d, *J* = 5.3 Hz, 2H), 3.57 (s, 2H), 3.55 (s, 8H), 3.51 – 3.47 (m, 2H), 3.10 (s, 1H). ^{13}C NMR (126 MHz, $CDCl_3$) δ 79.51, 74.60, 72.49, 70.45, 70.39, 70.36, 70.20, 70.14, 68.94, 61.45, 58.21.

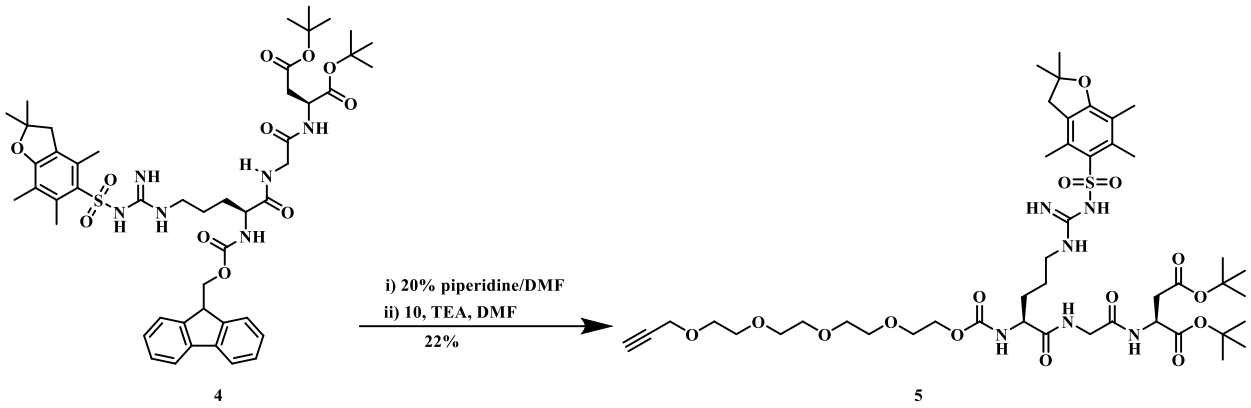
NMR data matched that in literature.[81]



Synthesis of 4-nitrophenyl(3,6,9,12-tetraoxapentadec-14-yn-1-yl) carbonate (10)

Compound **9** (0.2387 g, 1.028 mmol, 1eq) was dissolved with 10 mL dry dichloromethane in a 100 mL RBF under argon. Triethyl amine (TEA, 0.158 mL, 1.131 mmol, 1.1 eq) and 4-nitrophenyl chloroformate (0.2487 g, 1.234 mmol, 1.2 eq) was added to the solution, and stirred overnight at room temperature. Upon completion, the solvent was removed under reduced pressure, and the residual was dissolved with 20 mL ethyl acetate and poured into separatory funnel containing 30 mL of water. The aqueous layer was extracted with 3 × 25 mL ethyl acetate, and the combined organic layer was further washed with 5 × 50 mL water and 1 × 50 mL brine. After being dried over sodium sulfate, filtered, and concentrated under reduced pressure, the crude was subjected to silica gel column chromatography. Gradient elution from hexanes to 50% ethyl acetate-hexanes was used to obtain the product, **10**, as a brownish oil (0.25 g, 61% yield). R_f = 0.25 (50% Ethyl acetate-hexanes, potassium permanganate). ^{1}H NMR (500 MHz, $CDCl_3$) δ 8.25 (dd, *J* = 9.3, 2.9 Hz, 2H), 7.38 – 7.33 (m, 2H), 4.44 – 4.38 (m, 2H), 4.17 (t, *J* = 2.6 Hz, 2H),

3.79 (s, 2H), 3.66 (d, J = 10.3 Hz, 12H), 2.41 (d, J = 2.7 Hz, 1H). ^{13}C NMR (126 MHz, $CDCl_3$) δ 155.32, 152.27, 145.17, 125.09, 121.59, 79.46, 74.35, 70.49, 70.42, 70.20, 68.90, 68.40, 68.13, 58.17.

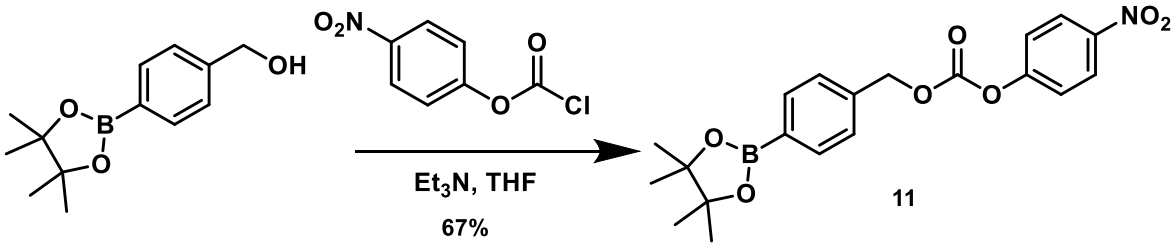


4 5

Synthesis of di-*tert*-butyl N^2-(2,5,8,11,14-pentaoxaheptadec-16-ynoyl)-N^{ω}-((2,2,4,6,7-pentamethyl-2,3-dihydrobenzofuran-5-yl)sulfonyl)arginylglycylaspartate (5)

Compounds **4** (0.0864 g, 0.093 mmol, 1 eq) was dissolved with 4 mL dry dimethylformamide in a 50 mL RBF under argon. After adding 0.8 mL piperidine, the reaction mixture was stirred at room temperature for 4 hours to yield a pale yellow solid. Next, the solvent was removed under reduced pressure and placed under hivac overnight to remove the residual solvent. Thereafter, compound **10** (0.044 g, 0.112 mmol, 1.2 eq) was added into the RBF under Argon, followed by addition of 3 mL of dry dimethylformamide and triethylamine (0.052 mL, 0.372 mmol, 4 eq). The solution was stirred at room temperature for 23 h. Upon completion, the solvent was removed under reduced pressure. The residual was re-dissolved with 15 mL dichloromethane and 15 mL water before transferring into the separatory funnel. The dichloromethane layer was collected, and the aqueous layer was extracted with 3 × 15 mL dichloromethane. The combined dichloromethane layer was further washed with 1 × 50 mL brine. After being dried over sodium sulfate, filtered, and concentrated under reduced pressure, the crude was then subjected to silica gel column chromatography. Gradient elution from dichloromethane-10% methanol-dichloromethane was used to obtain the product as a white solid (0.020 g, 22% yield). R_f = 0.6 (10% Methanol-Dichloromethane). ^{1}H NMR (500 MHz, $CDCl_3$) δ 7.68 (s, 1H), 7.16 (d, J = 8.2 Hz, 1H), 6.32 (s, 2H), 6.14 (s, 1H), 6.07 (s, 1H), 4.64 (d, J = 8.1 Hz, 1H), 4.29 (td, J = 8.1, 4.9

Hz, 1H), 4.17 (s, 4H), 4.04 – 3.90 (m, 2H), 3.69 – 3.60 (m, 14H), 3.29 (s, 1H), 3.18 (s, 1H), 2.94 (s, 2H), 2.78 (d, *J* = 4.9 Hz, 1H), 2.68 (dd, *J* = 16.9, 4.8 Hz, 1H), 2.57 (s, 3H), 2.50 (s, 3H), 2.45 (s, 1H), 2.24 (s, 1H), 2.08 (s, 3H), 1.90 (s, 1H), 1.71 (s, 1H), 1.59 (s, 2H), 1.44 (s, 6H), 1.41 (s, 18H). ^{13}C NMR (126 MHz, $CDCl_3$) δ 172.96, 170.21, 169.76, 169.37, 158.77, 156.66, 156.55, 138.48, 133.14, 132.41, 124.63, 117.52, 86.43, 82.60, 81.74, 79.72, 74.88, 70.57, 70.54, 70.39, 69.59, 69.15, 64.35, 58.46, 54.40, 49.48, 43.38, 42.92, 37.49, 29.90, 29.82, 28.72, 28.16, 27.99, 25.31, 19.41, 18.08, 12.60.

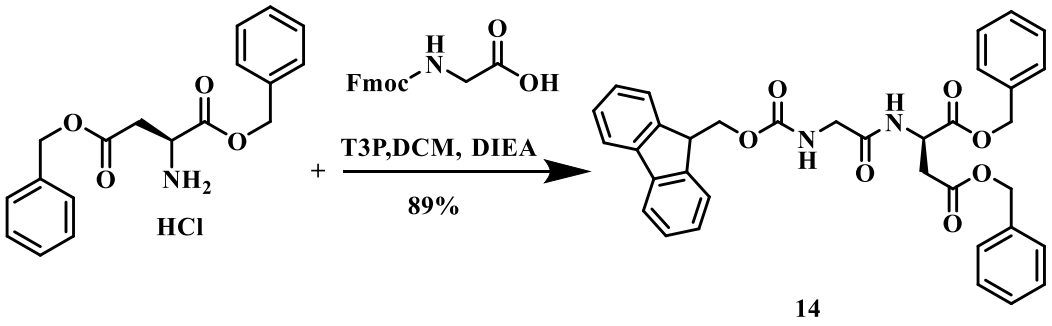


Synthesis of 4-nitrophenyl(4-(4,4,5,5-tetramethyl-1,3,2-dioxaborolan-2-yl)benzyl) carbonate (11)

In a 200 mL flask, (4-(4,4,5-tetramethyl-1,3,2-dioxaborolan-2-yl)phenyl)methanol (1 g, 4.27 mmol, 1 eq) was dissolved with 20 mL dry THF under argon at 0˚C. TEA (1.2 mL, 8.61 mmol, 2 eq) and 4-nitrophenyl chloroformate (0.94 g, 4.66 mmol, 1.1 eq) was added to the solution, and stirred overnight at room temperature. Solution turned yellow after the addition of 4-nitrophenyl chloroformate. Upon completion, the solvent was removed under reduced pressure, and the residual was dissolved with 20 mL ethyl acetate and poured into separatory funnel containing 25 mL of $NaHCO_3$. The aqueous layer was extracted with 3 × 25 mL ethyl acetate, and the combined organic layer was further washed with 5 × 50 mL water and 1 × 50 mL brine. After being dried over sodium sulfate, filtered, and concentrated under reduced pressure, the crude was subjected to silica gel column chromatography. Gradient elution from hexanes to 25% ethyl acetate-hexanes obtained the product as a white solid (1.14 g, 67% yield). R_f = 0.65 (50% Ethyl acetate-hexanes, UV, potassium permanganate). ^{1}H NMR (500 MHz, $CDCl_3$) δ 8.10 (d, *J* = 9.3 Hz, 2H), 7.74 (d, *J* = 8.1 Hz, 2H), 7.31 (d, *J* = 8.1 Hz, 2H), 7.24 (d, *J* = 9.3 Hz, 2H), 5.18 (s, 2H),

1.24 (s, 12H). ^{13}C NMR (126 MHz, $CDCl_3$) δ 155.22, 152.09, 145.07, 136.89, 134.74, 127.29, 124.94, 121.47, 83.82, 70.43, 24.57.

NMR data matched literature.[82]



14

In a 50 mL round-bottomed flask (RBF), di-*tert*-butyl L-Aspartate hydrochloride (0.14 g, 0.447, 1 eq) and fluorenylmethoxylcarbonyl glycine (0.133 g, 0.447 mmol, 1 eq) was dissolved with 10 ml of dry dichloromethane under argon gas with stirring. Afterwards, *N,N*-Diisopropylethylamine (DIEA, 0.152 mL, 0.894 mmol, 2 eq) was added. The solution was cooled in an ice-water bath to 0ºC and then propylphosphonic anhydride (T3P, 50 wt.% in ethyl acetate, 0.160 mL, 0.606 mmol, 1.2 eq) was added dropwise over 15 minutes. The ice-water bath was removed, and the reaction mixture was stirred for 24 hours. The reaction mixture was then quenched with water (3 mL), and poured into a separatory funnel containing 5 mL water. The aqueous layer was extracted with 2 × 15 mL dichloromethane, and the combined organic layer was further washed with 15 mL of saturated sodium hydrogen carbonate ($NaHCO_3$), 1 × 15 mL water, and 1 × 15 mL brine. The organic layer was dried over sodium sulfate, filtered and concentrated under reduced pressure to produce the product **14** as a white foam (0.24 g, 89 % yield). No further purification was required. R_f = 0.87 (9:1 dichloromethane/methanol, UV and potassium permanganate stain). ^{1}H NMR (500 MHz, $CDCl_3$) δ 7.71 (d, *J* = 7.5 Hz, 2H), 7.58 (d, *J* = 8.4 Hz, 2H), 7.35 (t, *J* = 7.6 Hz, 3H), 7.28 (d, *J* = 6.5 Hz, 4H), 7.26 – 7.20 (m, 7H), 5.88 (s, 1H), 5.12 – 5.03 (m, 3H), 5.02 – 4.93 (m, 3H), 4.35 (d, *J* = 7.5 Hz, 2H), 4.18 (t, *J* = 7.2 Hz, 1H), 3.92 (s, 2H), 3.04 (d, *J* = 17.2 Hz, 1H), 2.91 (d, *J* = 17.1 Hz, 1H). ^{13}C NMR (126 MHz, $CDCl_3$) δ

170.52, 170.25, 169.19, 156.56, 143.80, 143.78, 141.18, 135.24, 135.01, 128.49, 128.36, 128.32, 128.21, 128.13, 127.64, 127.02, 125.10, 119.90, 67.49, 67.16, 66.72, 48.71, 46.99, 44.19, 36.19.

References

(1) Large, D. E.; Abdelmessih, R. G.; Fink, E. A.; Auguste, D. T. Liposome composition in drug delivery design, synthesis, characterization, and clinical application. *Adv Drug Deliv Rev* **2021**, *176*, 113851. DOI: 10.1016/j.addr.2021.113851.

(2) Lima, P. H. C.; Butera, A. P.; Cabeca, L. F.; Ribeiro-Viana, R. M. Liposome surface modification by phospholipid chemical reactions. *Chem Phys Lipids* **2021**, *237*, 105084. DOI: 10.1016/j.chemphyslip.2021.105084.

(3) Liu, P.; Chen, G.; Zhang, J. A Review of Liposomes as a Drug Delivery System: Current Status of Approved Products, Regulatory Environments, and Future Perspectives. *Molecules* **2022**, *27* (4). DOI: 10.3390/molecules27041372.

(4) Priya, S.; Desai, V. M.; Singhvi, G. Surface Modification of Lipid-Based Nanocarriers: A Potential Approach to Enhance Targeted Drug Delivery. *ACS Omega* **2023**, *8* (1), 74-86. DOI: 10.1021/acsomega.2c05976.

(5) van Meer, G.; Voelker, D. R.; Feigenson, G. W. Membrane lipids: where they are and how they behave. *Nat Rev Mol Cell Biol* **2008**, *9* (2), 112-124. DOI: 10.1038/nrm2330 .

(6) Ren, H.; He, Y.; Liang, J.; Cheng, Z.; Zhang, M.; Zhu, Y.; Hong, C.; Qin, J.; Xu, X.; Wang, J. Role of Liposome Size, Surface Charge, and PEGylation on Rheumatoid Arthritis Targeting Therapy. *ACS Appl Mater Interfaces* **2019**, *11* (22), 20304-20315. DOI: 10.1021/acsami.8b22693.

(7) Pattni, B. S.; Chupin, V. V.; Torchilin, V. P. New Developments in Liposomal Drug Delivery. *Chem Rev* **2015**, *115* (19), 10938-10966. DOI: 10.1021/acs.chemrev.5b00046 .

(8) Berend.S, M. K. Phase Behavior of Model Lipid Bilayers. **2005**, *109*, 6553-6563.

(9) AlSawaftah, N.; Pitt, W. G.; Husseini, G. A. Dual-Targeting and Stimuli-Triggered Liposomal Drug Delivery in Cancer Treatment. *ACS Pharmacol Transl Sci* **2021**, *4* (3), 1028-1049. DOI: 10.1021/acsptsci.1c00066.

(10) Khan, M. I.; Hossain, M. I.; Hossain, M. K.; Rubel, M. H. K.; Hossain, K. M.; Mahfuz, A.; Anik, M. I. Recent Progress in Nanostructured Smart Drug Delivery Systems for Cancer Therapy: A Review. *ACS Appl Bio Mater* **2022**, *5* (3), 971-1012. DOI: 10.1021/acsabm.2c00002.

(11) Alshawwa, S. Z.; Kassem, A. A.; Farid, R. M.; Mostafa, S. K.; Labib, G. S. Nanocarrier Drug Delivery Systems: Characterization, Limitations, Future Perspectives and Implementation of Artificial Intelligence. *Pharmaceutics* **2022**, *14* (4). DOI: 10.3390/pharmaceutics14040883.
(12) Sun, L.; Liu, H.; Ye, Y.; Lei, Y.; Islam, R.; Tan, S.; Tong, R.; Miao, Y. B.; Cai, L. Smart nanoparticles for cancer therapy. *Signal Transduct Target Ther* **2023**, *8* (1), 418. DOI: 10.1038/s41392-023-01642-x.
(13) Lamichhane, N.; Udayakumar, T. S.; D'Souza, W. D.; Simone, C. B., 2nd; Raghavan, S. R.; Polf, J.; Mahmood, J. Liposomes: Clinical Applications and Potential for Image-Guided Drug Delivery. *Molecules* **2018**, *23* (2). DOI: 10.3390/molecules23020288.
(14) Garcia-Pinel, B.; Porras-Alcala, C.; Ortega-Rodriguez, A.; Sarabia, F.; Prados, J.; Melguizo, C.; Lopez-Romero, J. M. Lipid-Based Nanoparticles: Application and Recent Advances in Cancer Treatment. *Nanomaterials (Basel)* **2019**, *9* (4). DOI: 10.3390/nano9040638.
(15) Lee, H. Molecular Simulations of PEGylated Biomolecules, Liposomes, and Nanoparticles for Drug Delivery Applications. *Pharmaceutics* **2020**, *12* (6). DOI: 10.3390/pharmaceutics12060533.
(16) Alavi, M.; Hamidi, M. Passive and active targeting in cancer therapy by liposomes and lipid nanoparticles. *Drug Metab Pers Ther* **2019**, *34* (1). DOI: 10.1515/dmpt-2018-0032.
(17) De Leo, V.; Milano, F.; Agostiano, A.; Catucci, L. Recent Advancements in Polymer/Liposome Assembly for Drug Delivery: From Surface Modifications to Hybrid Vesicles. *Polymers (Basel)* **2021**, *13* (7). DOI: 10.3390/polym13071027.
(18) Riaz, M. K.; Riaz, M. A.; Zhang, X.; Lin, C.; Wong, K. H.; Chen, X.; Zhang, G.; Lu, A.; Yang, Z. Surface Functionalization and Targeting Strategies of Liposomes in Solid Tumor Therapy: A Review. *Int J Mol Sci* **2018**, *19* (1). DOI: 10.3390/ijms19010195.
(19) Josbert, M. M. P., B; Leo, W. T. B; Tom, V; Cor, S; Christien, O; Marca, H. M.W; Daan, J. A. C; Gert, S; Wim, E. H;. A Novel Family of L-Amino Acid-Based Biodegradable Polymer-Lipid Conjugates for the Development of Long-Circulating Liposomes with Effective Drug-Targeting Capacity *Bioconjugate Chem* **2003**, *14*, 1156-1164. DOI: 10.1021/bc0340363.
(20) Wang, R.; Xiao, R.; Zeng, Z.; Xu, L.; Wang, J. Application of poly(ethylene glycol)-distearoylphosphatidylethanolamine (PEG-DSPE) block copolymers and their derivatives as

nanomaterials in drug delivery. *Int J Nanomedicine* **2012**, *7*, 4185-4198. DOI: 10.2147/IJN.S34489.
(21) Bartheldyova, E.; Effenberg, R.; Masek, J.; Prochazka, L.; Knotigova, P. T.; Kulich, P.; Hubatka, F.; Velinska, K.; Zelnickova, J.; Zouharova, D.; et al. Hyaluronic Acid Surface Modified Liposomes Prepared via Orthogonal Aminoxy Coupling: Synthesis of Nontoxic Aminoxylipids Based on Symmetrically alpha-Branched Fatty Acids, Preparation of Liposomes by Microfluidic Mixing, and Targeting to Cancer Cells Expressing CD44. *Bioconjug Chem* **2018**, *29* (7), 2343-2356. DOI: 10.1021/acs.bioconjchem.8b00311.
(22) Song, M.; Liang, Y.; Li, K.; Zhang, J.; Zhang, N.; Tian, B.; Han, J. Hyaluronic acid modified liposomes for targeted delivery of doxorubicin and paclitaxel to CD44 overexpressing tumor cells with improved dual-drugs synergistic effect. *Journal of Drug Delivery Science and Technology* **2019**, *53*. DOI: 10.1016/j.jddst.2019.101179.
(23) Sercombe, L.; Veerati, T.; Moheimani, F.; Wu, S. Y.; Sood, A. K.; Hua, S. Advances and Challenges of Liposome Assisted Drug Delivery. *Front Pharmacol* **2015**, *6*, 286. DOI: 10.3389/fphar.2015.00286.
(24) Moulahoum, H.; Ghorbanizamani, F.; Zihnioglu, F.; Timur, S. Surface Biomodification of Liposomes and Polymersomes for Efficient Targeted Drug Delivery. *Bioconjug Chem* **2021**, *32* (8), 1491-1502. DOI: 10.1021/acs.bioconjchem.1c00285 .
(25) Manjappa, A. S.; Chaudhari, K. R.; Venkataraju, M. P.; Dantuluri, P.; Nanda, B.; Sidda, C.; Sawant, K. K.; Murthy, R. S. Antibody derivatization and conjugation strategies: application in preparation of stealth immunoliposome to target chemotherapeutics to tumor. *J Control Release* **2011**, *150* (1), 2-22. DOI: 10.1016/j.jconrel.2010.11.002.
(26) Holliger, P.; Hudson, P. J. Engineered antibody fragments and the rise of single domains. *Nat Biotechnol* **2005**, *23* (9), 1126-1136. DOI: 10.1038/nbt1142.
(27) Alshaer, W.; Hillaireau, H.; Vergnaud, J.; Ismail, S.; Fattal, E. Functionalizing Liposomes with anti-CD44 Aptamer for Selective Targeting of Cancer Cells. *Bioconjug Chem* **2015**, *26* (7), 1307-1313. DOI: 10.1021/bc5004313.
(28) Sato, Y.; Asawa, K.; Huang, T.; Noiri, M.; Nakamura, N.; Ekdahl, K. N.; Nilsson, B.; Ishihara, K.; Teramura, Y. Induction of Spontaneous Liposome Adsorption by Exogenous

Surface Modification with Cell-Penetrating Peptide-Conjugated Lipids. *Langmuir* **2021**, *37* (32), 9711-9723. DOI: 10.1021/acs.langmuir.1c01072.
(29) Zhang, L.; Shan, X.; Meng, X.; Gu, T.; Guo, L.; An, X.; Jiang, Q.; Ge, H.; Ning, X. Novel Integrin alphavbeta3-Specific Ligand for the Sensitive Diagnosis of Glioblastoma. *Mol Pharm* **2019**, *16* (9), 3977-3984. DOI: 10.1021/acs.molpharmaceut.9b00602 .
(30) Humphries, J. D.; Byron, A.; Humphries, M. J. Integrin ligands at a glance. *J Cell Sci* **2006**, *119* (Pt 19), 3901-3903. DOI: 10.1242/jcs.03098.
(31) Fu, S.; Zhao, Y.; Sun, J.; Yang, T.; Zhi, D.; Zhang, E.; Zhong, F.; Zhen, Y.; Zhang, S.; Zhang, S. Integrin alpha(v)beta(3)-targeted liposomal drug delivery system for enhanced lung cancer therapy. *Colloids Surf B Biointerfaces* **2021**, *201*, 111623. DOI: 10.1016/j.colsurfb.2021.111623.
(32) Desgrosellier, J. S.; Cheresh, D. A. Integrins in cancer: biological implications and therapeutic opportunities. *Nat Rev Cancer* **2010**, *10* (1), 9-22. DOI: 10.1038/nrc2748 .
(33) Wu, Y. J.; Pagel, M. A.; Muldoon, L. L.; Fu, R.; Neuwelt, E. A. High alphav Integrin Level of Cancer Cells Is Associated with Development of Brain Metastasis in Athymic Rats. *Anticancer Res* **2017**, *37* (8), 4029-4040. DOI: 10.21873/anticanres.11788.
(34) Friedrich, E. B.; Liu, E.; Sinha, S.; Cook, S.; Milstone, D. S.; MacRae, C. A.; Mariotti, M.; Kuhlencordt, P. J.; Force, T.; Rosenzweig, A.; et al. Integrin-linked kinase regulates endothelial cell survival and vascular development. *Mol Cell Biol* **2004**, *24* (18), 8134-8144. DOI: 10.1128/MCB.24.18.8134-8144.2004.
(35) Valdembri, D.; Sandri, C.; Santambrogio, M.; Serini, G. Regulation of integrins by conformation and traffic: it takes two to tango. *Mol Biosyst* **2011**, *7* (9), 2539-2546. DOI: 10.1039/c1mb05066d.
(36) Cleaver, O. M., D.A. Endothelial signaling during development. *Nature medicine* **2003**, *9*, 6.
(37) Shattil, S. J.; Kim, C.; Ginsberg, M. H. The final steps of integrin activation: the end game. *Nat Rev Mol Cell Biol* **2010**, *11* (4), 288-300. DOI: 10.1038/nrm2871 .
(38) Pierschbacher, M. D.; Ruoslahti, E.; Sundelin, J.; Lind, P.; Peterson, P. A. The cell attachment domain of fibronectin. Determination of the primary structure. *Journal of Biological Chemistry* **1982**, *257* (16), 9593-9597. DOI: 10.1016/s0021-9258(18)34113-9.

(39) Pierschbacher, M. D. R., E. Cell attachment activity of fibronectin can be duplicated by small synthetic fragments of the molecule. *Nature* **1984**, *309*, 30-33.
(40) Pierschbacher, M. D. R., E. Variants of the cell recognition site of fibronectin that retain attachment-promoting activity. *Proc.Natl.Acad.Sci.U.S.A* **1984**, *81*, 5985-5988.
(41) Battistini, L.; Bugatti, K.; Sartori, A.; Curti, C.; Zanardi, F. RGD Peptide-Drug Conjugates as Effective Dual Targeting Platforms: Recent Advances. *European Journal of Organic Chemistry* **2021**, *2021* (17), 2506-2528. DOI: 10.1002/ejoc.202100240.
(42) Chang, M. W.; Lo, J. M.; Juan, H. F.; Chang, H. Y.; Chuang, C. Y. Combination of RGD compound and low-dose paclitaxel induces apoptosis in human glioblastoma cells. *PLoS One* **2012**, *7* (5), e37935. DOI: 10.1371/journal.pone.0037935.
(43) Chen, C.; Duan, Z.; Yuan, Y.; Li, R.; Pang, L.; Liang, J.; Xu, X.; Wang, J. Peptide-22 and Cyclic RGD Functionalized Liposomes for Glioma Targeting Drug Delivery Overcoming BBB and BBTB. *ACS Appl Mater Interfaces* **2017**, *9* (7), 5864-5873. DOI: 10.1021/acsami.6b15831.
(44) Cossu, J.; Thoreau, F.; Boturyn, D. Multimeric RGD-Based Strategies for Selective Drug Delivery to Tumor Tissues. *Pharmaceutics* **2023**, *15* (2). DOI: 10.3390/pharmaceutics15020525.
(45) Li, W.; Su, B.; Meng, S.; Ju, L.; Yan, L.; Ding, Y.; Song, Y.; Zhou, W.; Li, H.; Tang, L.; et al. RGD-targeted paramagnetic liposomes for early detection of tumor: in vitro and in vivo studies. *Eur J Radiol* **2011**, *80* (2), 598-606. DOI: 10.1016/j.ejrad.2011.01.051.
(46) Song, Z.; Lin, Y.; Zhang, X.; Feng, C.; Lu, Y.; Gao, Y.; Dong, C. Cyclic RGD peptide-modified liposomal drug delivery system for targeted oral apatinib administration: enhanced cellular uptake and improved therapeutic effects. *Int J Nanomedicine* **2017**, *12*, 1941-1958. DOI: 10.2147/IJN.S125573.
(47) Sun, Y.; Li, X.; Zhang, L.; Liu, X.; Jiang, B.; Long, Z.; Jiang, Y. Cell Permeable NBD Peptide-Modified Liposomes by Hyaluronic Acid Coating for the Synergistic Targeted Therapy of Metastatic Inflammatory Breast Cancer. *Mol Pharm* **2019**, *16* (3), 1140-1155. DOI: 10.1021/acs.molpharmaceut.8b01123.
(48) Amin, M.; Mansourian, M.; Koning, G. A.; Badiee, A.; Jaafari, M. R.; Ten Hagen, T. L. M. Development of a novel cyclic RGD peptide for multiple targeting approaches of liposomes to tumor region. *J Control Release* **2015**, *220* (Pt A), 308-315. DOI: 10.1016/j.jconrel.2015.10.039.

(49) Zhang, Y. F.; Wang, J. C.; Bian, D. Y.; Zhang, X.; Zhang, Q. Targeted delivery of RGD-modified liposomes encapsulating both combretastatin A-4 and doxorubicin for tumor therapy: in vitro and in vivo studies. *Eur J Pharm Biopharm* **2010**, *74* (3), 467-473. DOI: 10.1016/j.ejpb.2010.01.002.
(50) Ye, H.; Zhou, Y.; Liu, X.; Chen, Y.; Duan, S.; Zhu, R.; Liu, Y.; Yin, L. Recent Advances on Reactive Oxygen Species-Responsive Delivery and Diagnosis System. *Biomacromolecules* **2019**, *20* (7), 2441-2463. DOI: 10.1021/acs.biomac.9b00628 .
(51) Abdal Dayem, A.; Hossain, M. K.; Lee, S. B.; Kim, K.; Saha, S. K.; Yang, G. M.; Choi, H. Y.; Cho, S. G. The Role of Reactive Oxygen Species (ROS) in the Biological Activities of Metallic Nanoparticles. *Int J Mol Sci* **2017**, *18* (1). DOI: 10.3390/ijms18010120.
(52) Lou, J.; Qualls, M. L.; Best, M. D. Sticking the Landing: Enhancing Liposomal Cell Delivery using Reversible Covalent Chemistry and Caged Targeting Groups. *Chembiochem* **2023**, *24* (2), e202200436. DOI: 10.1002/cbic.202200436.
(53) Saravanakumar, G.; Kim, J.; Kim, W. J. Reactive-Oxygen-Species-Responsive Drug Delivery Systems: Promises and Challenges. *Adv Sci (Weinh)* **2017**, *4* (1), 1600124. DOI: 10.1002/advs.201600124.
(54) Murphy, M. P. How mitochondria produce reactive oxygen species. *Biochem J* **2009**, *417* (1), 1-13. DOI: 10.1042/BJ20081386.
(55) Bedard, K.; Krause, K. H. The NOX family of ROS-generating NADPH oxidases: physiology and pathophysiology. *Physiol Rev* **2007**, *87* (1), 245-313. DOI: 10.1152/physrev.00044.2005.
(56) Tahara, E. B.; Navarete, F. D.; Kowaltowski, A. J. Tissue-, substrate-, and site-specific characteristics of mitochondrial reactive oxygen species generation. *Free Radic Biol Med* **2009**, *46* (9), 1283-1297. DOI: 10.1016/j.freeradbiomed.2009.02.008.
(57) Okado-Matsumoto, A.; Fridovich, I. Subcellular distribution of superoxide dismutases (SOD) in rat liver: Cu,Zn-SOD in mitochondria. *J Biol Chem* **2001**, *276* (42), 38388-38393. DOI: 10.1074/jbc.M105395200.
(58) Sosa, V.; Moline, T.; Somoza, R.; Paciucci, R.; Kondoh, H.; ME, L. L. Oxidative stress and cancer: an overview. *Ageing Res Rev* **2013**, *12* (1), 376-390. DOI: 10.1016/j.arr.2012.10.004.

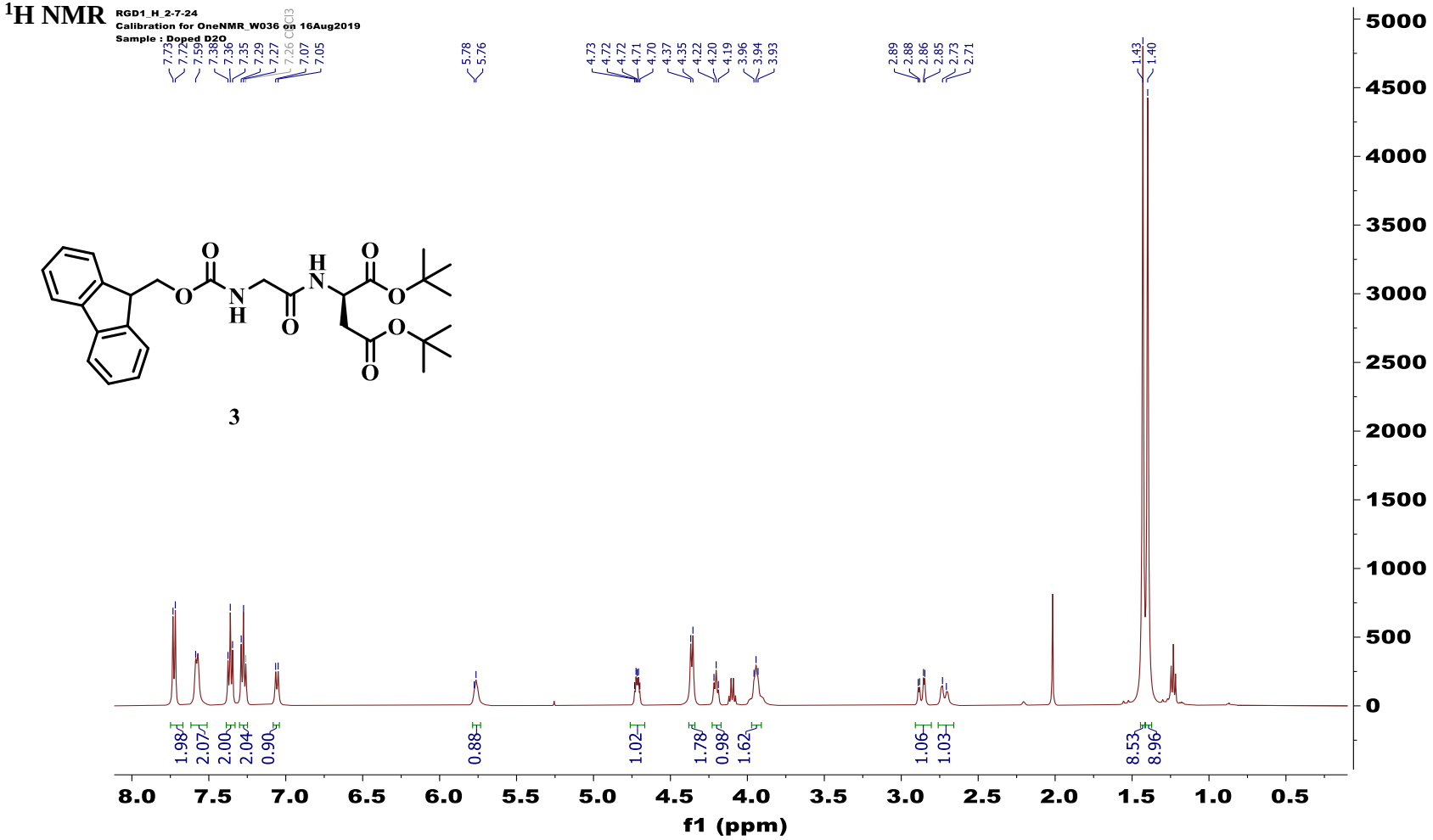
(59) Wu, H.; Yin, J. J.; Wamer, W. G.; Zeng, M.; Lo, Y. M. Reactive oxygen species-related activities of nano-iron metal and nano-iron oxides. *J Food Drug Anal* **2014**, *22* (1), 86-94. DOI: 10.1016/j.jfda.2014.01.007.
(60) Mura, S.; Nicolas, J.; Couvreur, P. Stimuli-responsive nanocarriers for drug delivery. *Nat Mater* **2013**, *12* (11), 991-1003. DOI: 10.1038/nmat3776.
(61) Valko, M.; Rhodes, C. J.; Moncol, J.; Izakovic, M.; Mazur, M. Free radicals, metals and antioxidants in oxidative stress-induced cancer. *Chem Biol Interact* **2006**, *160* (1), 1-40. DOI: 10.1016/j.cbi.2005.12.009.
(62) Finkel, T. Signal transduction by reactive oxygen species. *J Cell Biol* **2011**, *194* (1), 7-15. DOI: 10.1083/jcb.201102095.
(63) Tao, W.; He, Z. ROS-responsive drug delivery systems for biomedical applications. *Asian J Pharm Sci* **2018**, *13* (2), 101-112. DOI: 10.1016/j.ajps.2017.11.002.
(64) Kataoka, K.; Harada, A.; Nagasaki, Y. Block copolymer micelles for drug delivery: Design, characterization and biological significance. *Advanced Drug Delivery Reviews* **2012**, *64*, 37-48. DOI: 10.1016/j.addr.2012.09.013.
(65) Gong, J.; Chen, M.; Zheng, Y.; Wang, S.; Wang, Y. Polymeric micelles drug delivery system in oncology. *J Control Release* **2012**, *159* (3), 312-323. DOI: 10.1016/j.jconrel.2011.12.012.
(66) Ma, N. L., Y; Xu, H; Wang, Z; Zhang, X. Dual Redox Responsive Assemblies Formed from Diselenide Block Copolymers. *J. Am.Chem.Soc* **2010**, *132*, 442-443.
(67) Han, P.; Li, S.; Cao, W.; Li, Y.; Sun, Z.; Wang, Z.; Xu, H. Red light responsive diselenide-containing block copolymer micelles. *J Mater Chem B* **2013**, *1* (6), 740-743. DOI: 10.1039/c2tb00186a.
(68) Broaders, K. E.; Grandhe, S.; Frechet, J. M. A biocompatible oxidation-triggered carrier polymer with potential in therapeutics. *J Am Chem Soc* **2011**, *133* (4), 756-758. DOI: 10.1021/ja110468v.
(69) Accardo, A.; Morelli, G. Review peptide-targeted liposomes for selective drug delivery: Advantages and problematic issues. *Biopolymers* **2015**, *104* (5), 462-479. DOI: 10.1002/bip.22678.

(70) van der Koog, L.; Gandek, T. B.; Nagelkerke, A. Liposomes and Extracellular Vesicles as Drug Delivery Systems: A Comparison of Composition, Pharmacokinetics, and Functionalization. *Adv Healthc Mater* **2022**, *11* (5), e2100639. DOI: 10.1002/adhm.202100639.
(71) Chen, L.; Liu, Y.; Wang, W.; Liu, K. Effect of integrin receptor-targeted liposomal paclitaxel for hepatocellular carcinoma targeting and therapy. *Oncol Lett* **2015**, *10* (1), 77-84. DOI: 10.3892/ol.2015.3242.
(72) Gandek, T. B., van der Koog, L., Nagelkerke, A., . A Comparison of Cellular Uptake Mechanisms, Delivery Efficacy, and Intracellular Fate between Liposomes and Extracellular Vesicles. *Adv. Healthcare Mater* **2023**, *12*, 2300319.
(73) Lou, J.; Best, M. D. Reactive Oxygen Species-Responsive Liposomes via Boronate-Caged Phosphatidylethanolamine. *Bioconjug Chem* **2020**, *31* (9), 2220-2230. DOI: 10.1021/acs.bioconjchem.0c00397.
(74) Lou, J.; Qualls, M. L.; Hudson, M. M.; McBee, D. P.; Baccile, J. A.; Best, M. D. Reactive Oxygen Species (ROS) Activated Liposomal Cell Delivery using a Boronate-Caged Guanidine Lipid. *Chemistry* **2022**, *28* (46), e202201057. DOI: 10.1002/chem.202201057.
(75) Du, Y.; He, W.; Xia, Q.; Zhou, W.; Yao, C.; Li, X. Thioether Phosphatidylcholine Liposomes: A Novel ROS-Responsive Platform for Drug Delivery. *ACS Appl Mater Interfaces* **2019**, *11* (41), 37411-37420. DOI: 10.1021/acsami.9b08901.
(76) Liu, J.; Wu, Z.; Liu, Y.; Zhan, Z.; Yang, L.; Wang, C.; Jiang, Q.; Ran, H.; Li, P.; Wang, Z. ROS-responsive liposomes as an inhaled drug delivery nanoplatform for idiopathic pulmonary fibrosis treatment via Nrf2 signaling. *J Nanobiotechnology* **2022**, *20* (1), 213. DOI: 10.1186/s12951-022-01435-4.
(77) Lippert, A. R., Van de Bittner, G.C. and Chang, C.J.,. Boronate Oxidation as a Bioorthogonal Reaction Approach for Studying the Chemistry of Hydrogen Peroxide in Living Systems. *Accounts of chemical research* **2011**, *44* (9), 793-804.
(78) O'Neil E. J, D. K. M., Smith B.D. Phosphatidylcholine-Derived Bolaamphiphiles via Click Chemistry. *org.Lett* **2007**, *9*, 199-202.
(79) Babiker E, G. M., Garfield P. R, and Gary E. M. Removal of benzyl type protecting groups from peptides by catalytic transfer hydrogenation with formic acid. *J.org.chem* **1979**, *44* (19), 3442-3444.

(80) Welsh, D. J.; Smith, D. K. Comparing dendritic and self-assembly strategies to multivalency--RGD peptide-integrin interactions. *Org Biomol Chem* **2011**, *9* (13), 4795-4801. DOI: 10.1039/c1ob05241a.
(81) Aeschi, Y.; Drayss-Orth, S.; Valášek, M.; Raps, F.; Häussinger, D.; Mayor, M. Assembly of [2]Rotaxanes in Water. *European Journal of Organic Chemistry* **2017**, *2017* (28), 4091-4103. DOI: 10.1002/ejoc.201700640.
(82) Li, J.; Li, Y.; He, Q.; Li, Y.; Li, H.; Liu, L. One-pot native chemical ligation of peptide hydrazides enables total synthesis of modified histones. *Org Biomol Chem* **2014**, *12* (29), 5435-5441. DOI: 10.1039/c4ob00715h.

Appendix

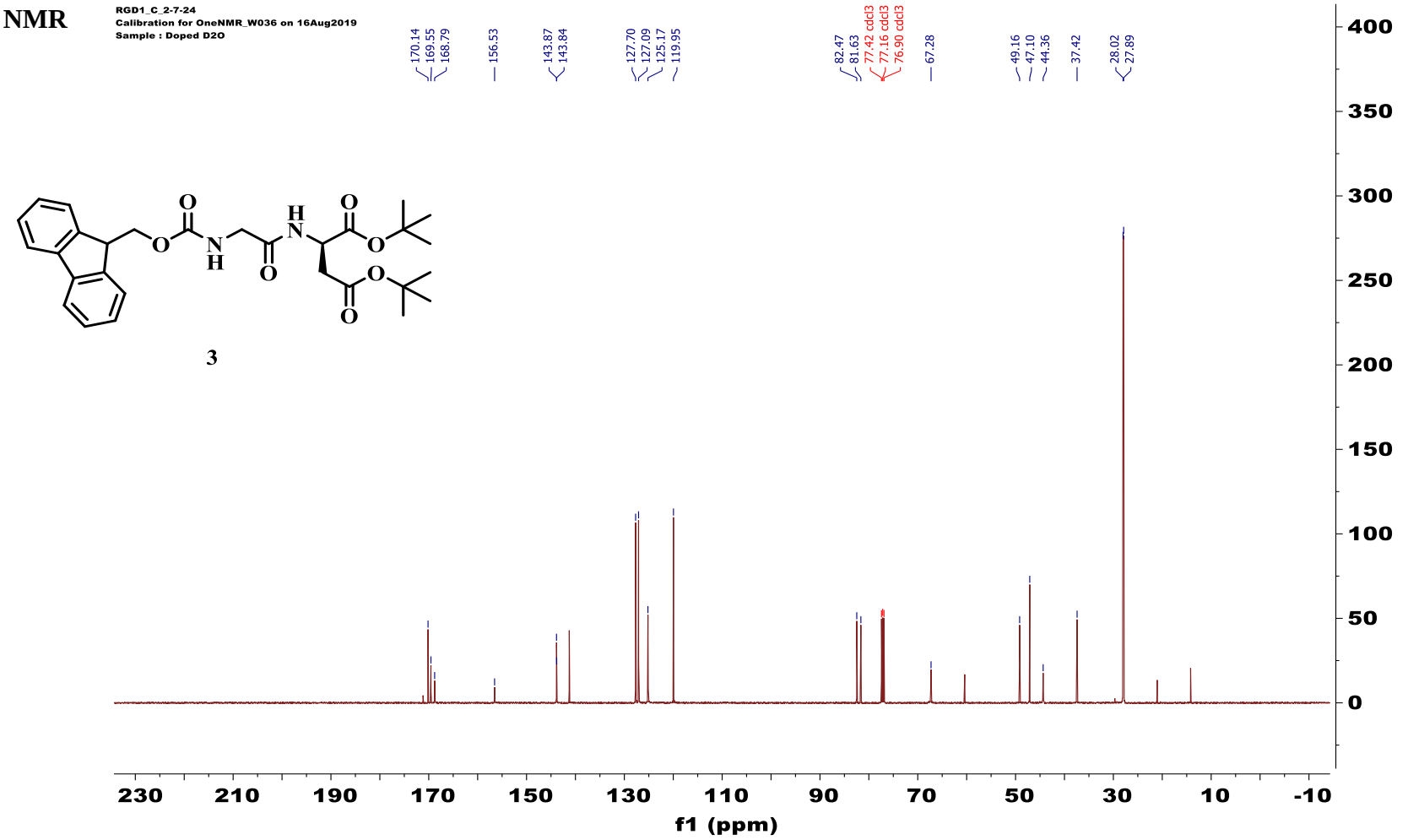
^{1}H NMR



3

Figure 3.1: ^{1}H NMR of 3

^{13}C NMR



3

Figure 3.2: ^{13}C NMR of 3

^{1}H NMR

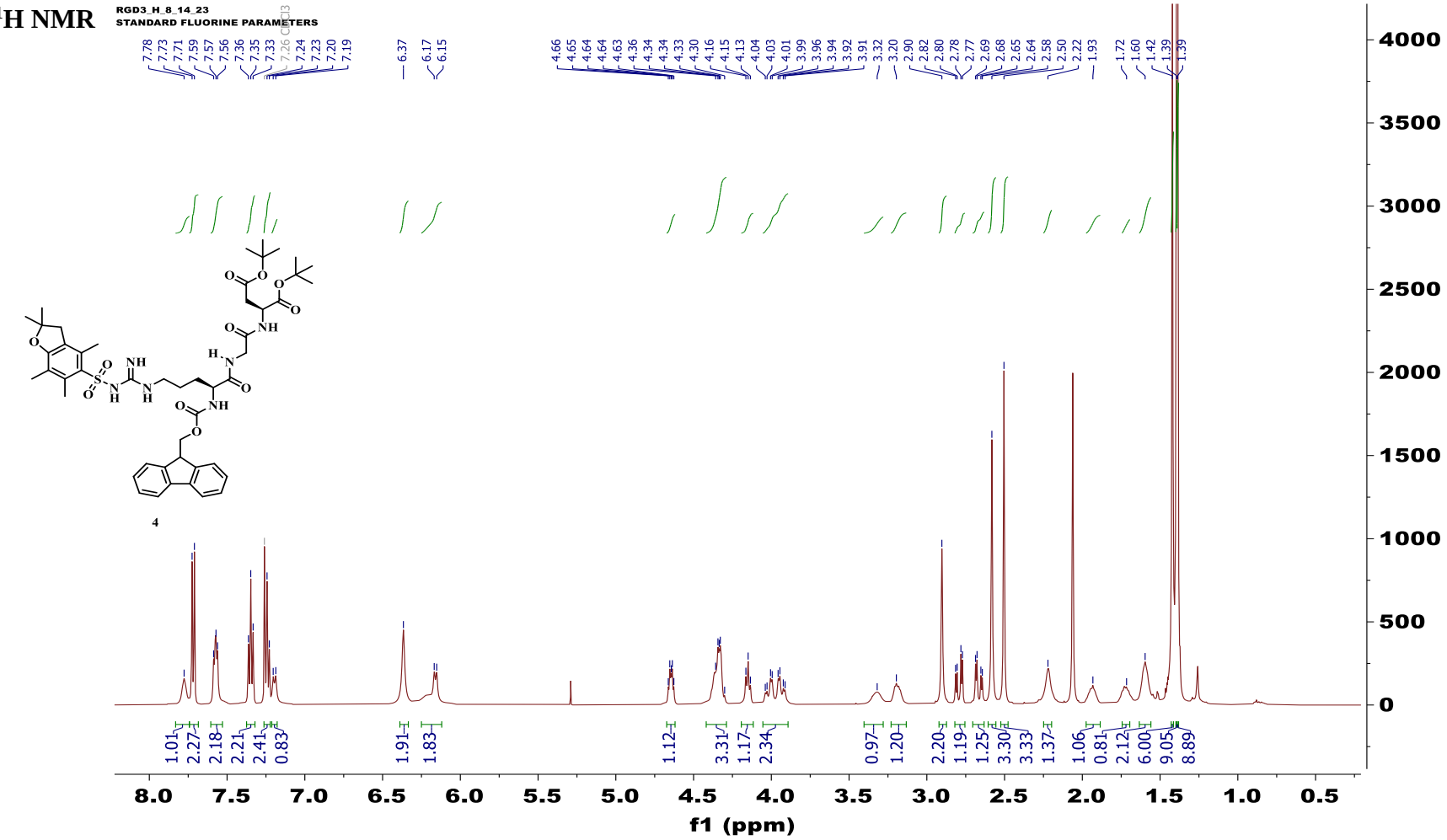


Figure 3.3: ^{1}H NMR of 4

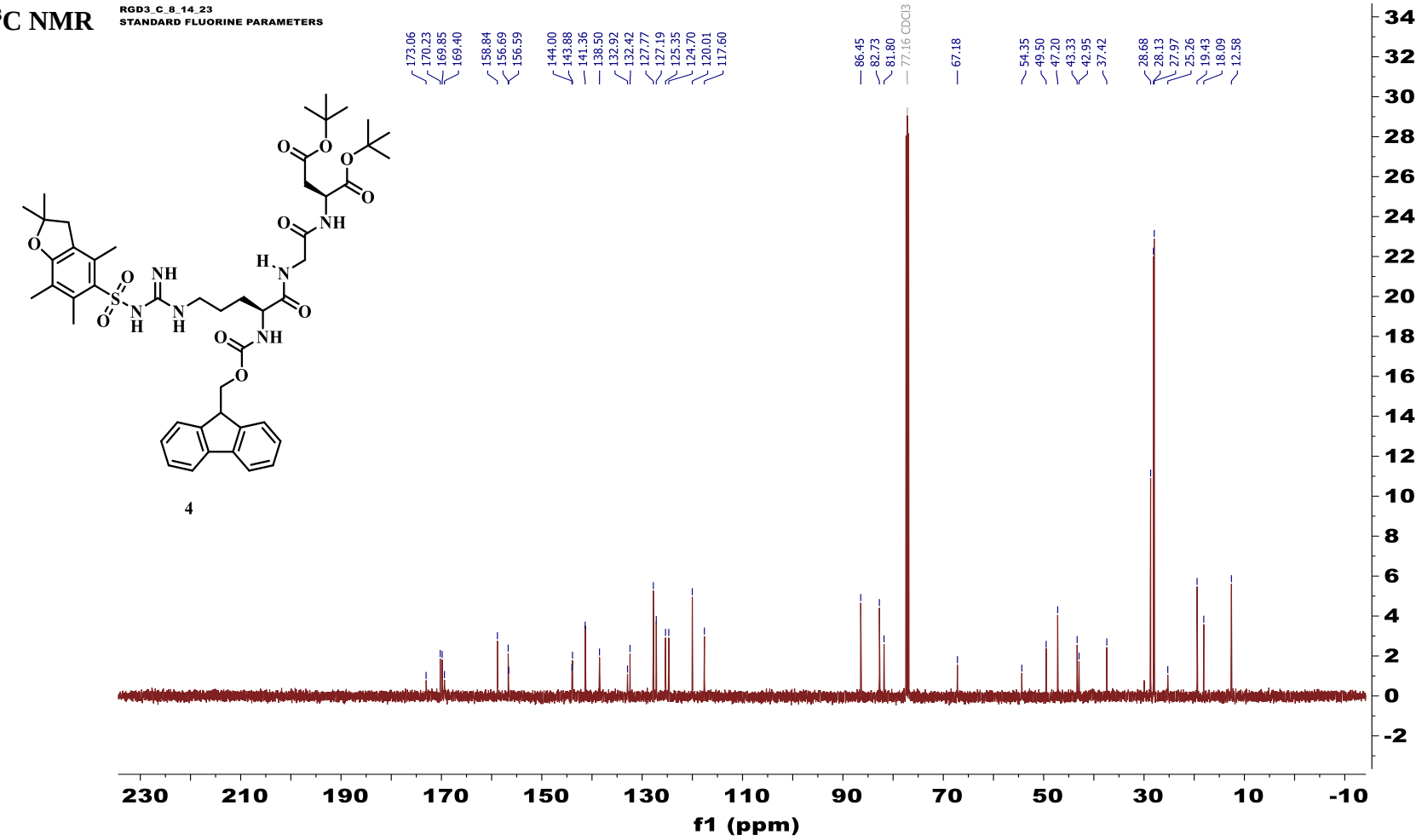


Figure 3.4: ^{13}C NMR of 4

^{1}H NMR

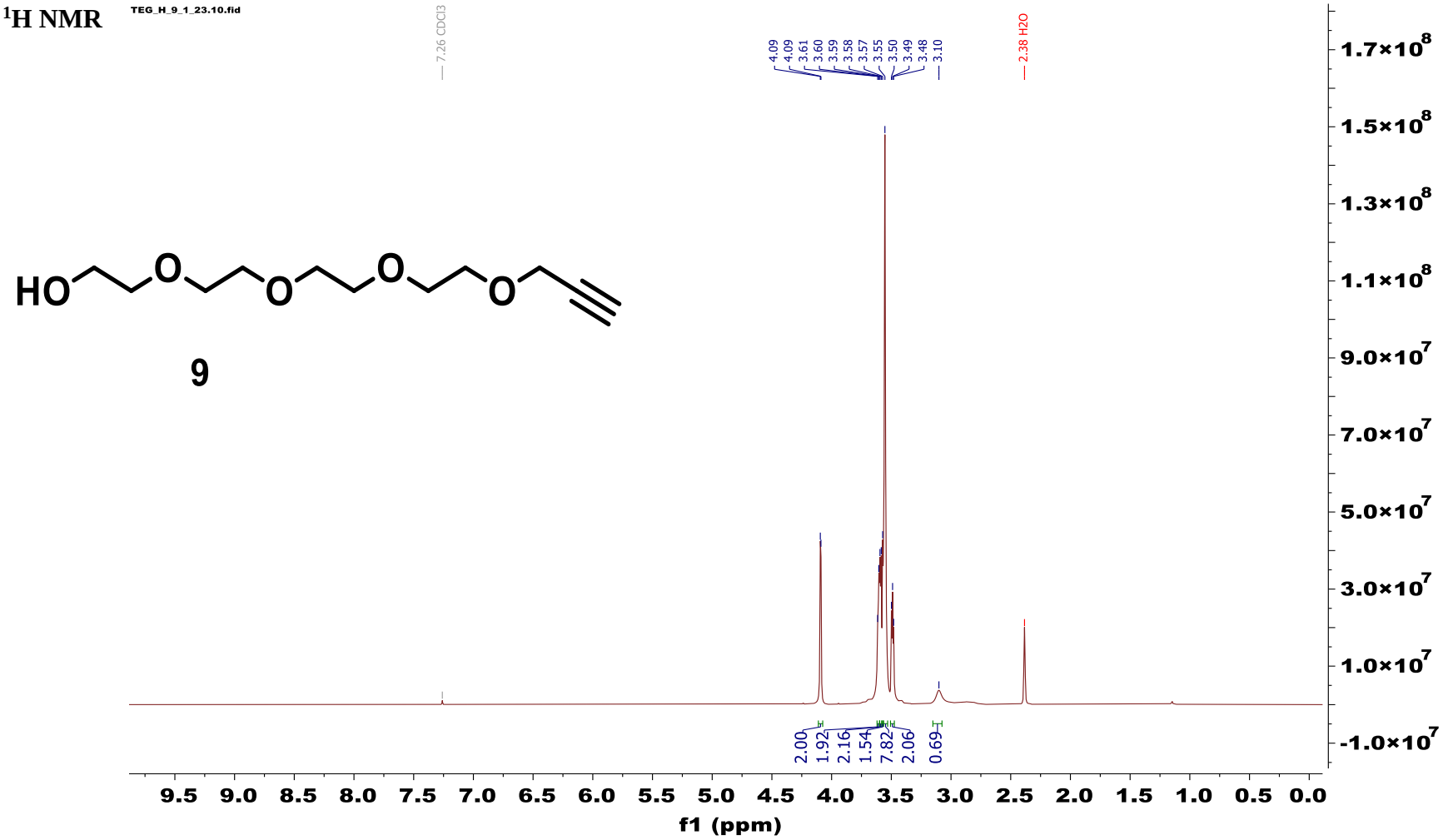


Figure 3.5: ^{1}H NMR of 9

^{13}C NMR

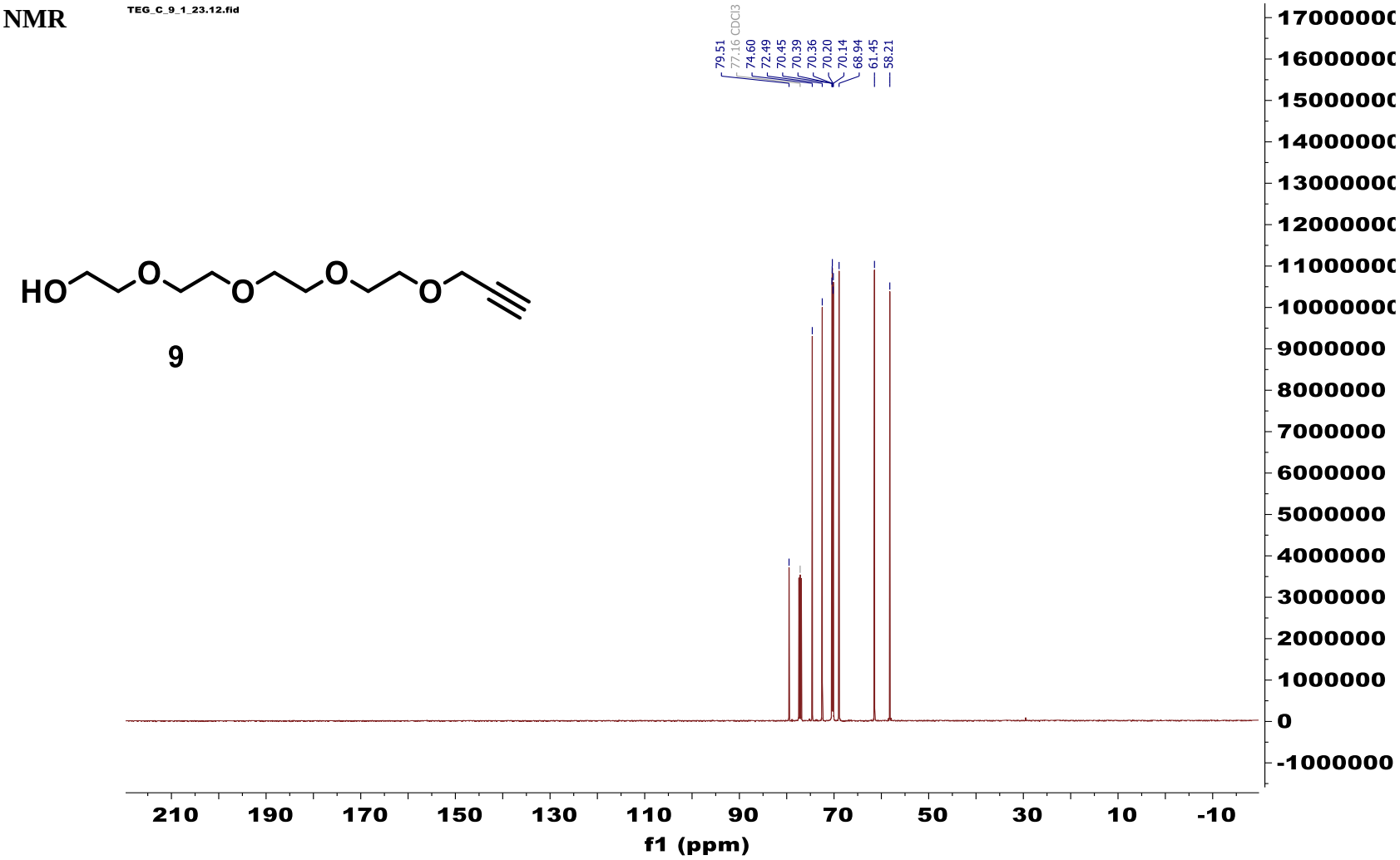


Figure 3.6: ^{13}C NMR of 9

^{1}H NMR

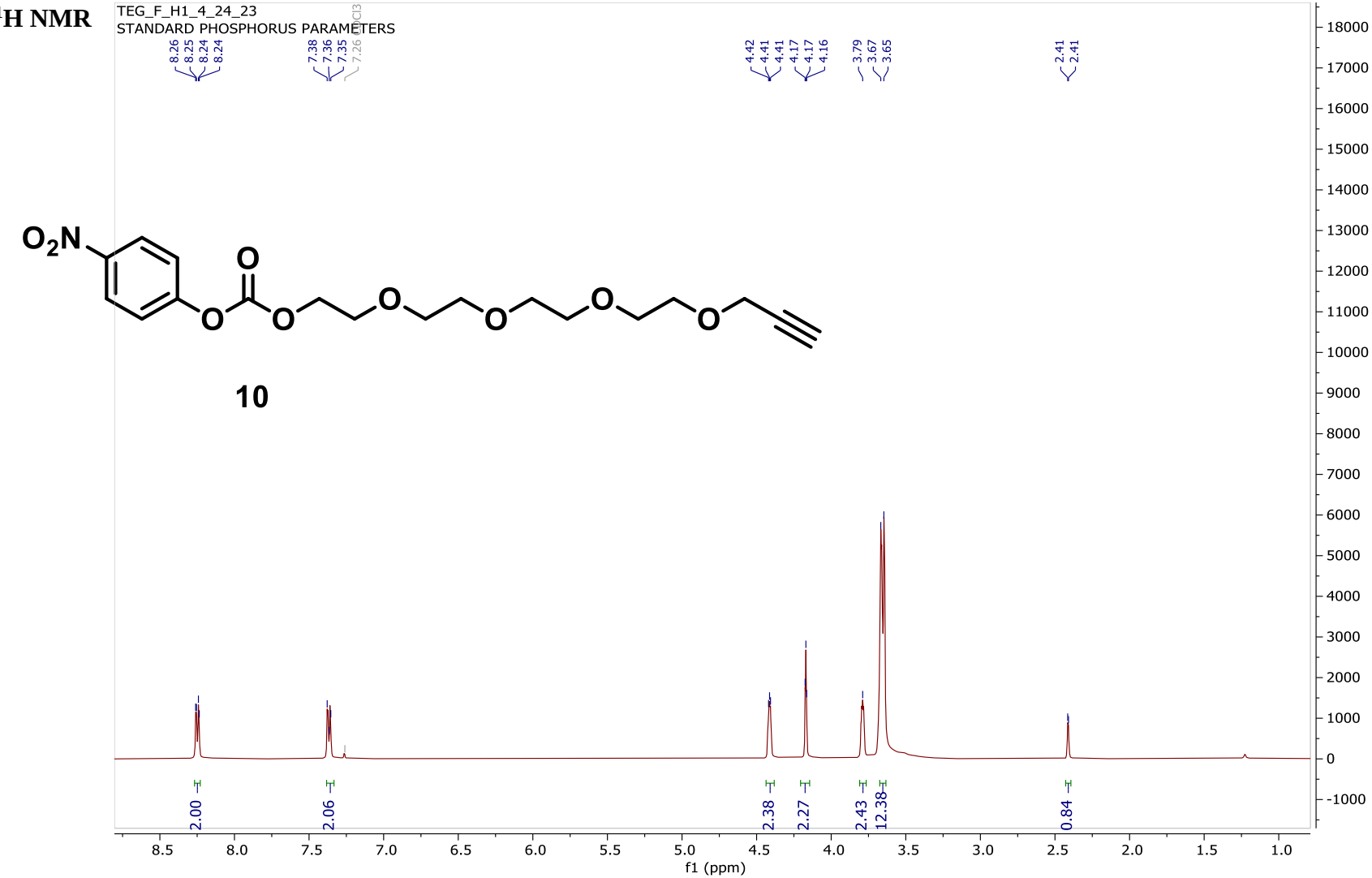


Figure 3.7: ^{1}H NMR of 10

^{13}C NMR

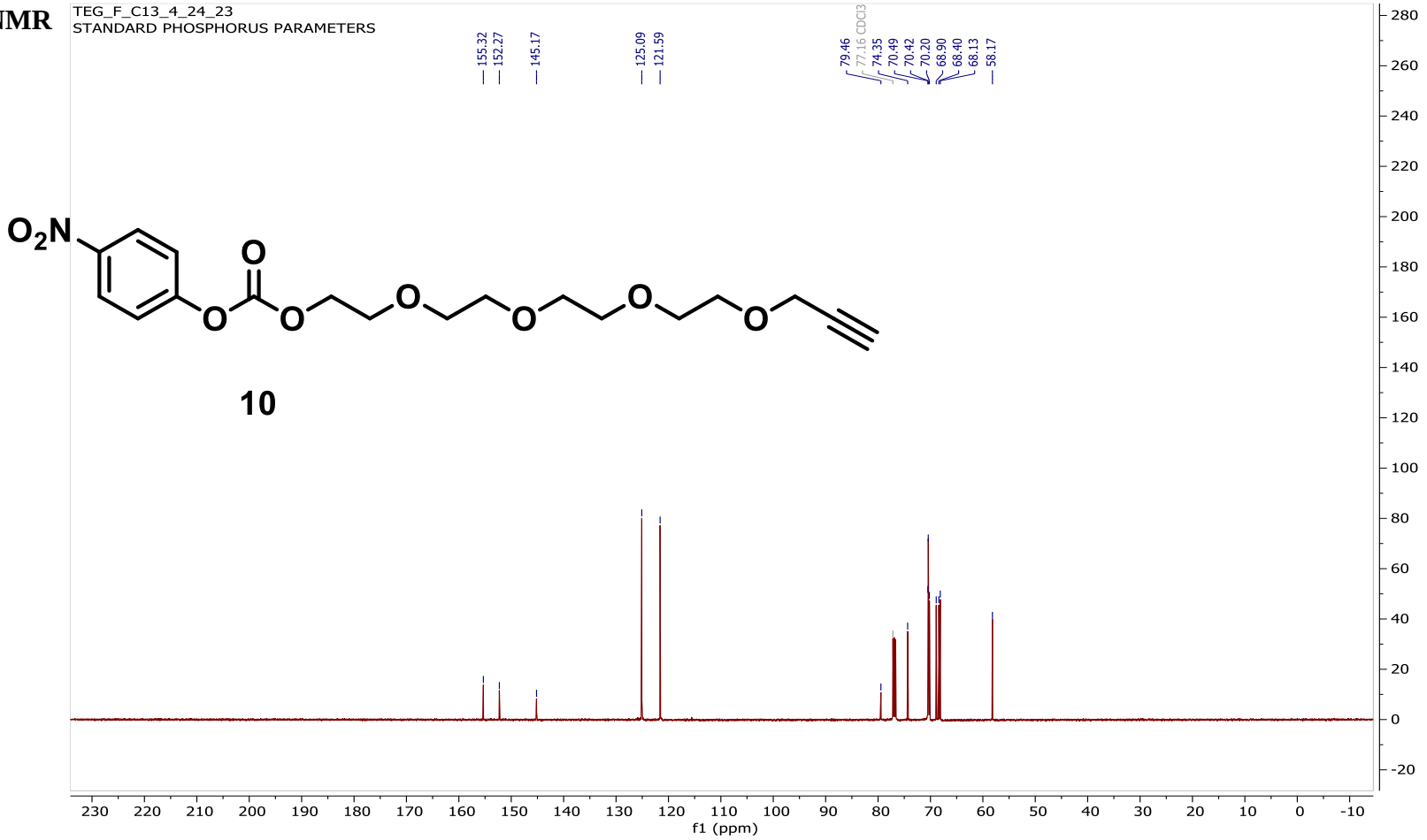


Figure 3.8: ^{13}C NMR of 10

^{1}H NMR

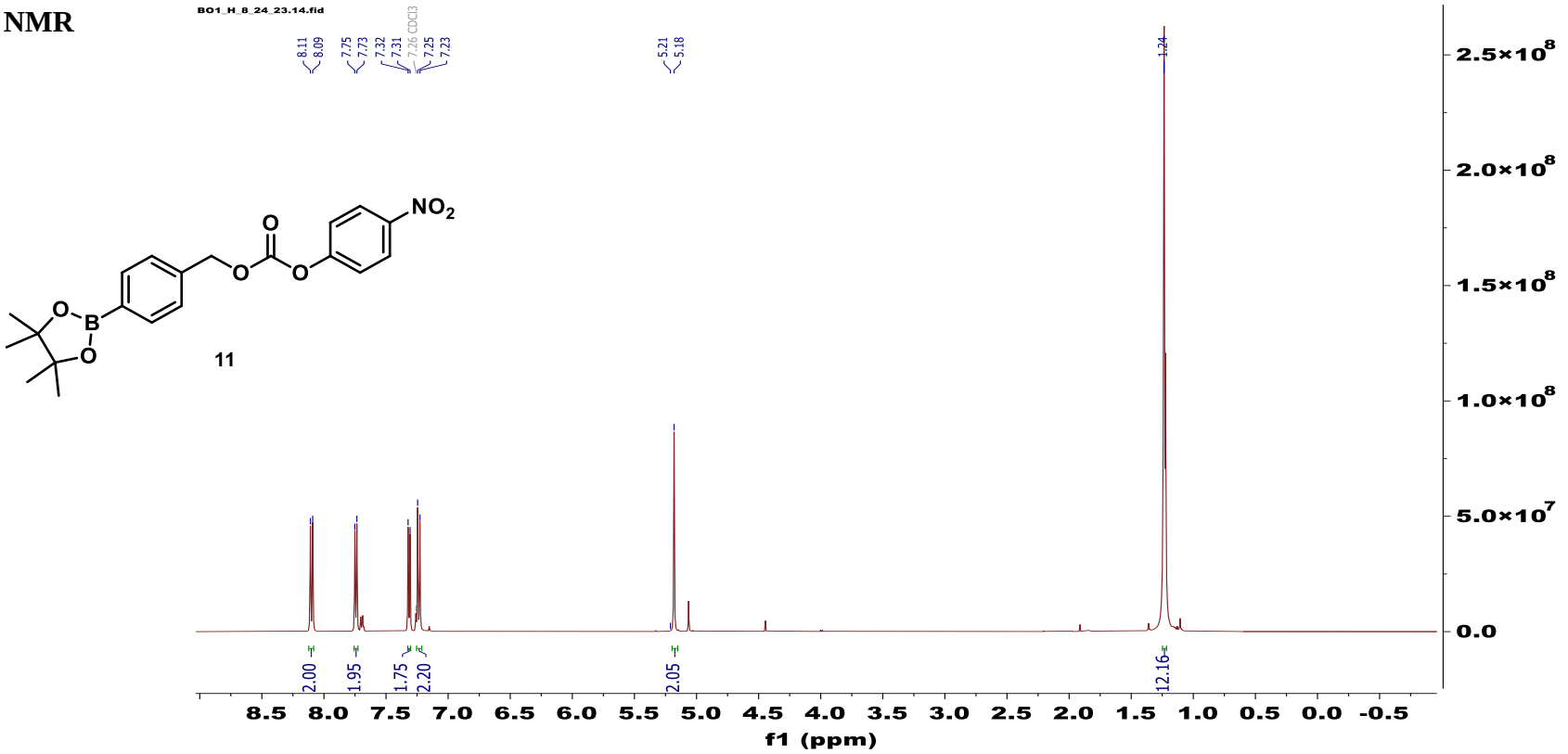


Figure 3.9: ^{1}H NMR of 11

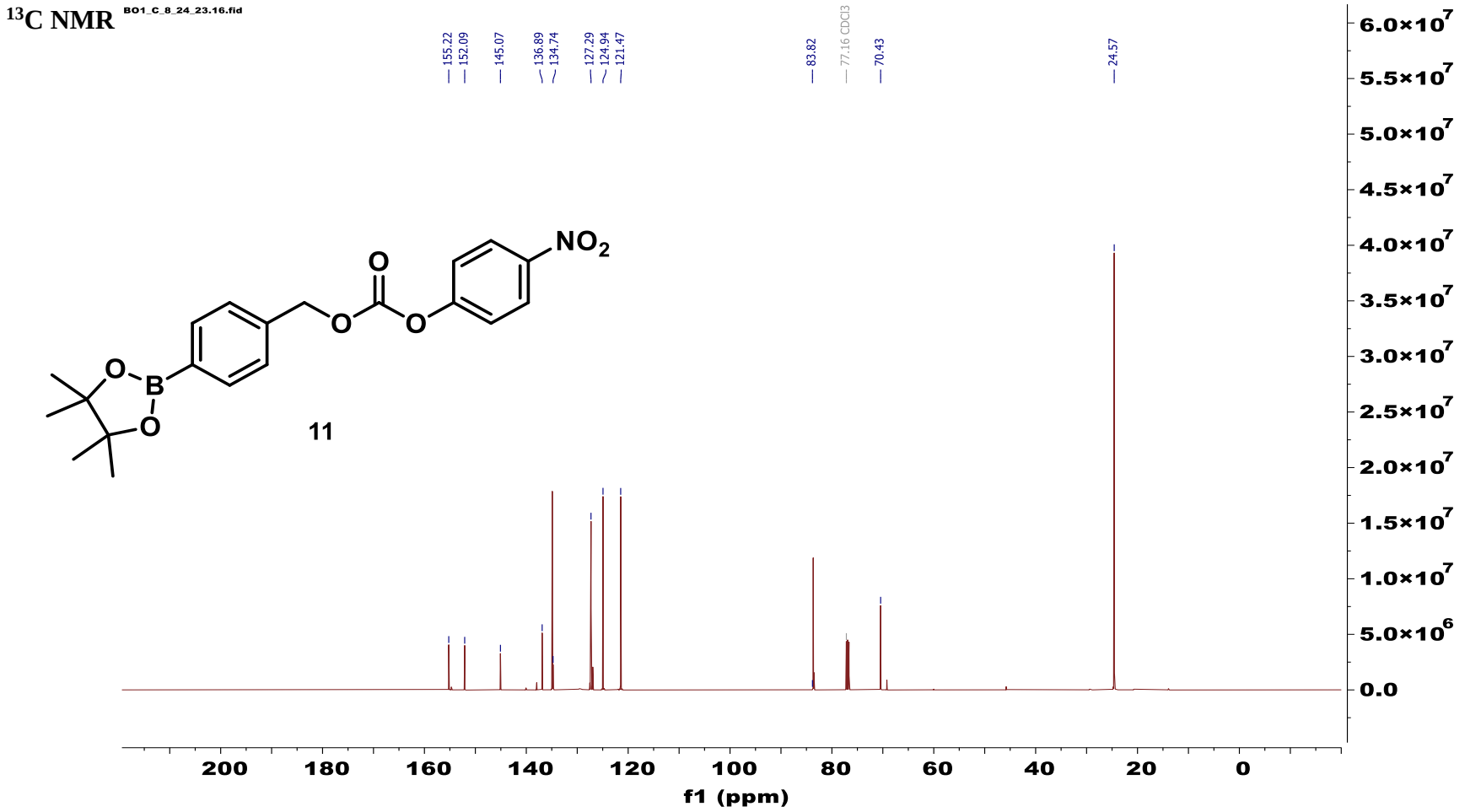


Figure 3.10: ^{13}C NMR of 11

^{1}H NMR

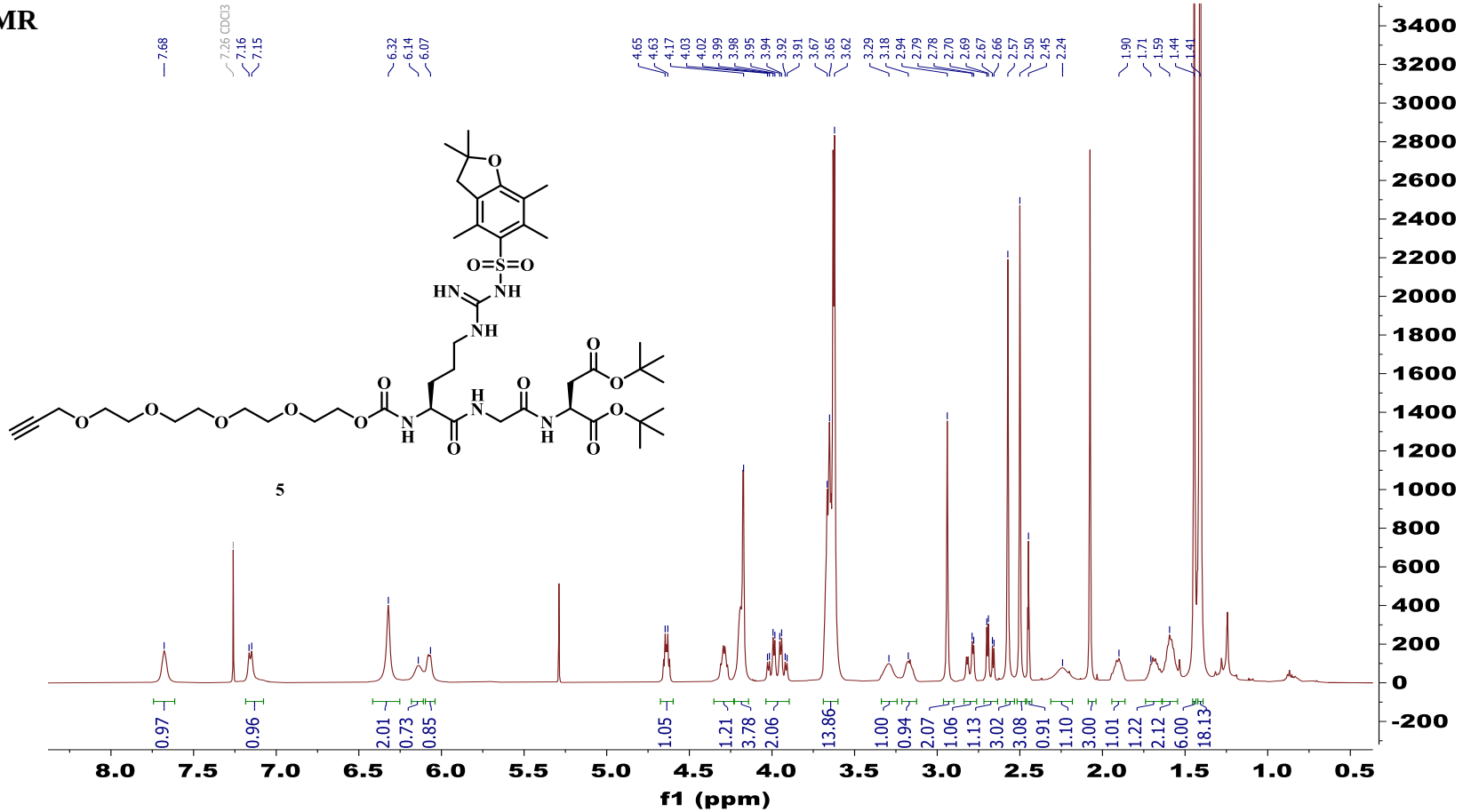


Figure 3.11: ^{1}H NMR of 5

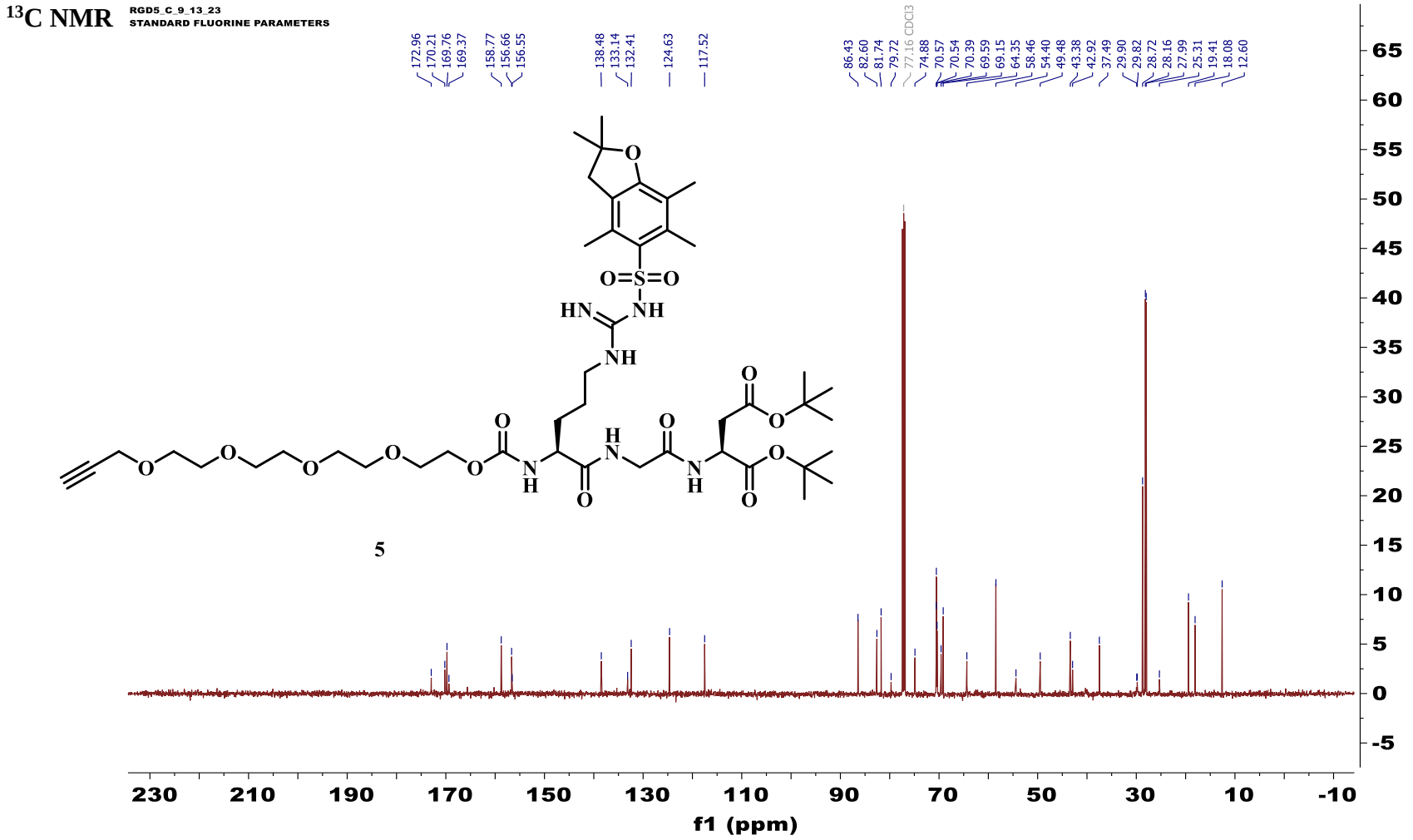


Figure 3.12: ^{13}C NMR of 5

^{1}H NMR

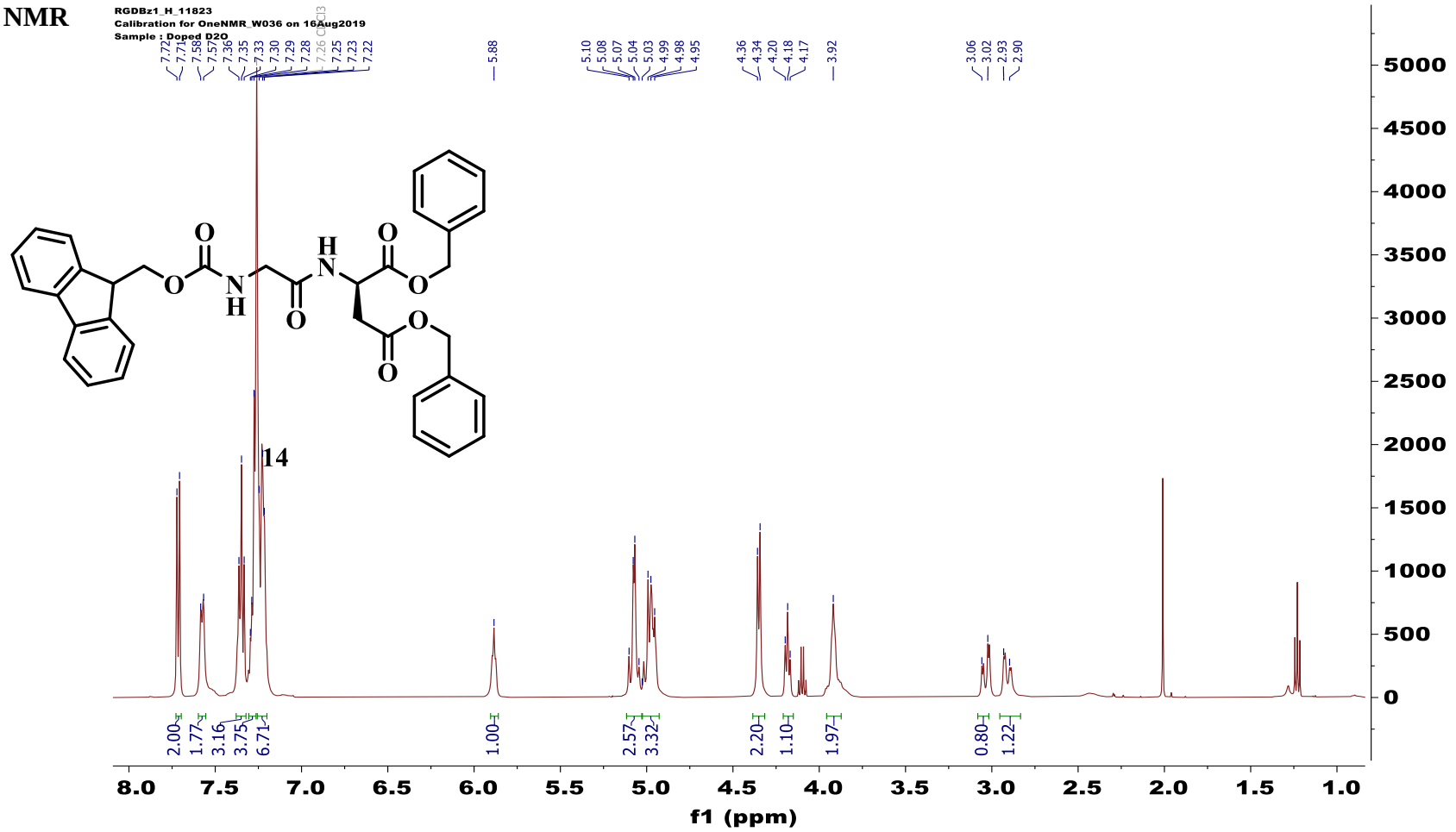


Figure 3.13: ^{1}H NMR of 14

^{13}C NMR

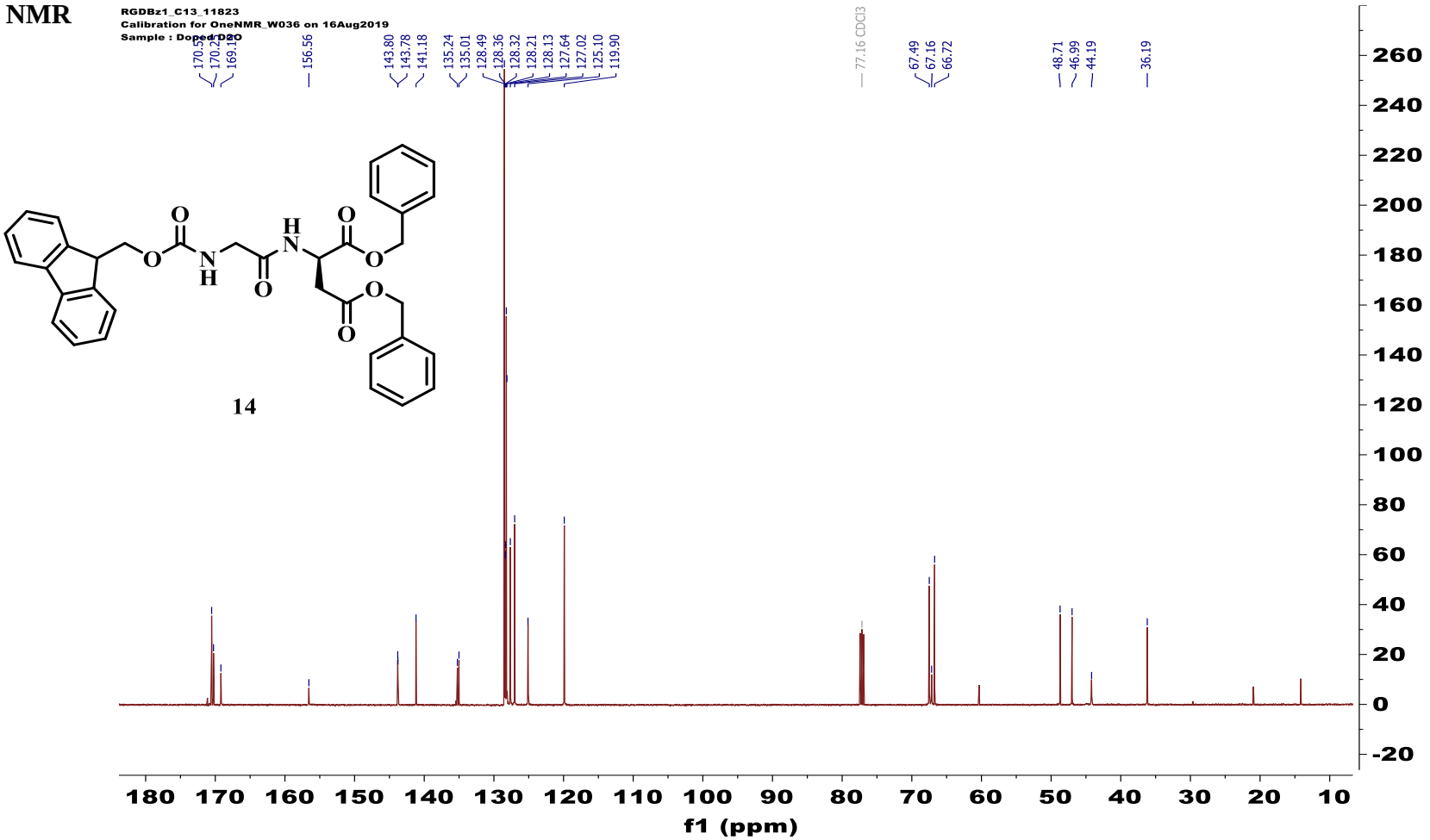


Figure 3.14: ^{13}C NMR of 14

Vita

Michael Kadiri was born and raised in Lagos, Nigeria. In 2019, he earned a Bachelor of Science degree in Chemistry from the University of Ibadan. In 2022, he began his graduate studies at the University of Tennessee, Knoxville, where he joined Dr. Best's lab and contributed to the synthesis of ROS-responsive RGD lipids.